Accepted Manuscript

Multi-proxy isotopic tracing of magmatic sources and crustal recycling in the Palaeozoic to early Jurassic active margin of North-Western Gondwana

Roelant van der Lelij, Richard Spikings, Axel Gerdes, Massimo Chiaradia, Torsten Vennemann, Andrés Mora

PII: S1342-937X(18)30267-3
DOI: https://doi.org/10.1016/j.gr.2018.09.007
Reference: GR 2040

To appear in: *Gondwana Research*

Received date: 4 May 2018
Revised date: 28 September 2018
Accepted date: 28 September 2018

Please cite this article as: Roelant van der Lelij, Richard Spikings, Axel Gerdes, Massimo Chiaradia, Torsten Vennemann, Andrés Mora , Multi-proxy isotopic tracing of magmatic sources and crustal recycling in the Palaeozoic to early Jurassic active margin of North-Western Gondwana. Gr (2018), https://doi.org/10.1016/j.gr.2018.09.007

Multi-proxy isotopic tracing of magmatic sources and crustal recycling in the Palaeozoic to Early Jurassic active margin of North-Western Gondwana

Roelant van der Lelij[1], Richard Spikings[2], Axel Gerdes[3], Massimo Chiaradia[2], Torsten Vennemann[4] and Andrés Mora[5]

[1] Geological Survey of Norway, PO Box 6315 Sluppen, 7491 Trondheim, Norway

[2] Department of Earth Sciences, University of Geneva, Rue des Maraichers 13, 1205 Geneva, Switzerland

[3]Institut für Geowissenschaften, Facheinheit Mineralogie – Petrologie und Geochemie, Goethe Universität Frankfurt, Altenhöferallee 1, D-60438 Frankfurt am Main, Germany

[4]Institute of Mineralogy and Geochemistry, University of Lausanne, CH-1015 Lausanne, Switzerland

[5]Instituto Colombiano del Petróleo, Ecopetrol, Bucaramanga, Colombia

Abstract

We trace source variations of active margin granitoids which crystallised intermittently over ~300 Ma in varying kinematic regimes, by combining zircon Lu-Hf isotopic data from Early Palaeozoic to Early Jurassic igneous and metaigneous rocks in the Mérida Andes, Venezuela and the Santander Massif, Colombia, with new whole rock Rb/Sr and Sm-Nd isotopic data, and quartz O isotopic data. These new data are unique in South America because they were obtained from discrete magmatic and metamorphic zircon populations, providing a high temporal resolution dataset, and compare several isotopic systems on the same samples. Collectively, these data provide valuable insight into the evolution of the isotopic structure of the continental crust in long-lived active margins.

Phanerozoic active margin-related granitoids in the Mérida Andes and the Santander Massif yield zircon Lu-Hf model ages ranging between 0.77 Ga and 1.57 Ga which clearly define temporal trends that can be correlated with changes in tectonic regimes. The oldest Lu-Hf model ages of >1.3 Ga are restricted to granitoids which formed during Barrovian metamorphism and crustal thickening between ~499 Ma and ~473 Ma. These granitoids yield high initial $^{87}Sr/^{86}Sr$ ratios, suggesting that evolved, Rb-rich middle to upper crust was the major source of melt. Granitoids and rhyolites which crystallised during subsequent extension between ~472 Ma and ~452 Ma yield younger Lu-Hf model ages of 0.80 Ga – 1.3 Ga and low initial $^{87}Sr/^{86}Sr$ ratios, suggesting that they were derived from much more juvenile, Rb-poor sources such as mafic lower crust and mantle-derived melts. The rapid change in magmatic sources at ~472 Ma can be attributed either to reduced crustal assimilation during extension, or a short pulse of crustal growth by addition of juvenile material to the continental crust. Between ~472 Ma and ~196 Ma Lu-Hf model ages remain mostly constant between ~1.0 and ~1.2 Ga. The large scatter and the absence of definite trends in initial $^{87}Sr/^{86}Sr$ ratios suggest that both mafic, Rb-poor, and evolved Rb-rich sources were important precursors of active margin magmas in Colombia and Venezuela throughout the Palaeozoic to the Early Jurassic.

Previous studies have shown that the genesis of arc magmas may be stimulated by heat advection to the crust during the underplating of mantle derived melt, but the absence of permanent younging trends in Lu-Hf model ages from ~472 Ma to ~196 Ma suggests that very little new crust was generated during this period in the studied region. An overwhelming majority of the analysed igneous rocks yield zircon Lu-Hf model ages of > 1 Ga which may be accounted for by documented local crustal end members of 1 Ga - 1.6 Ga, and do not require contributions from the depleted mantle. Therefore, recycling of ~1 Ga and older crust was a dominant process in the north-western corner of Gondwana between ~472 Ma and ~196 Ma.

This study shows that whole rock Sm-Nd and zircon Lu-Hf data can be interpreted similarly regarding the age of the source regions, whereas Rb-Sr and O isotope data from the same rocks yield valuable information regarding the geochemical nature of the source.

1. Introduction

There is no consensus on the timing or the mechanisms which lead to the formation and growth of the Earth's continental crust. Some models argue that the present day volume of continental crust formed in the Archaean, and that it has subsequently remained stable or diminished (e.g. Fyfe, 1978; Armstrong, 1991; Stern and Scholl, 2010). Other models argue for ongoing episodic crustal growth in extensional active margins during slab retreat (e.g. Hawkesworth and Kemp, 2006; Kemp et al., 2009; Collins et al., 2011), during which heat advection in the continental crust may be driven by the addition of mantle derived melt to the overriding plate, resulting in the observed variety of arc magma compositions (e.g. Huppert and Sparks, 1988; Petford et al., 2000; Annen et al., 2006). However, episodic growth at active continental margins may be compensated by subduction erosion, resulting in overall net loss since at least the beginning of the Jurassic (e.g. Clift and Vannucchi, 2004; Stern and Scholl, 2010). This study investigates crustal growth along the active margin of north-western Gondwana, during ~300 million years of intermittent active margin magmatism (Van der Lelij et al., 2016b) between the Early Palaeozoic and Early Jurassic.

Ocean-continent interaction along western Gondwana formed the Andean mountain belt, which spans an along-strike distance of >7500 km (e.g. Gutscher, 2002). Active margin magmatism in the Andes is documented throughout the Phanerozoic, with several temporal gaps (e.g. the Devonian; Bahlburg et al., 2009). Most studies of Palaeozoic and Mesozoic zircons from western South America reveal a paucity of Lu-Hf model ages that are <1 Ga (Augustsson et al., 2006; Willner et al., 2008; Bahlburg et al., 2009; Mišković and Schaltegger, 2009; Reimann et al., 2010; Hauser et al., 2011), indicating that Paleozoic to Mesozoic rocks which formed on the

western margin of Gondwana mainly recycled ~1 Ga and older continental lithosphere. Significant exceptions are late Palaeozoic to Mesozoic arc rocks in Peru (Boekhout et al., 2015), and Early Cretaceous arc rocks in western Colombia and Ecuador (Cochrane et al., 2014b), where crustal growth is documented by net contributions of 30-45% and ~60% of juvenile, mantle derived material, respectively, during periods of arc extension. Therefore, crustal growth in an active continental margin is partly dependant on regional kinematics, which can vary drastically over along-strike distances of 100 km (Gutscher, 2002; Ramos, 2009).

The Santander Massif of Colombia and the adjacent Mérida Andes of Venezuela (Fig. 1) host numerous active margin granitoids with concordant zircon U-Pb ages that span between 499 and ~196 Ma (Table 1). These granitoids bracket documented periods of crustal thickening and extension driven by varying subduction zone kinematics (Van der Lelij et al., 2016b). Investigating how these kinematics evolve in time and space, and how they are linked with magmatic processes are relevant to understanding crustal growth and recycling at active margins.

Zircon Lu-Hf and whole rock Sm-Nd data can provide insights into the time of melt extraction from the mantle (e.g. Hawkesworth and Kemp, 2006). Rb-Sr data are more sensitive to source rock type because Rb is an incompatible element and thus Rb rich source rocks tend to be K-feldspar and mica rich rocks which may have formed in the upper crust (e.g. Rollinson, 1993). Similarly, oxygen tends to be enriched in heavier isotopes in rocks which were exposed to meteoric water, and therefore granitoids hosting quartz with $\delta^{18}O > 12$ ‰ may be derived from partial melting of sedimentary protoliths (e.g. Harris et al., 1997). We present Lu-Hf isotopic data from zircons extracted from 52 igneous and metamorphic rocks collected from the Santander Massif of Colombia and the Mérida Andes of Venezuela, which we combine with new whole rock Sm-Nd and Rb-Sr isotopic data and quartz O isotopic data. We use these data to evaluate the age and nature of melt sources, their relationship to geodynamic settings and the implications for crustal growth and recycling along the western margin of Gondwana.

2. Regional setting

The Maracaibo Block (Fig.1) forms part of the South Caribbean Plate Boundary Zone, and is separated from the Bonaire Block to the north via a regional dextral strike slip fault zone that exposes isolated basement fragments (e.g. Toas Island; Fig. 1). East-west oriented compression during the Cainozoic (e.g. Hoorn et al., 1995; Bermúdez et al., 2011; Villagómez et al., 2011) formed the high elevation of the Colombian Santander Massif (~4400 m) and the Venezuelan Mérida Andes (4978 m) (Fig. 1), which host numerous exposures of Precambrian and Palaeozoic metamorphic and igneous basement in the south-eastern and western boundaries of the Maracaibo Block.

Precambrian basement is documented in inliers in the Sierra Nevada de Santa Marta, the Garzón Massif and in boreholes of the Llanos basin (Fig. 1), which yield zircon U-Pb ages between ~1.8 Ga and ~1 Ga (Cordani et al., 2005; Ibañez-Mejia et al., 2011). These Precambrian rocks may have formed within island arcs and accreted to the Amazonian Craton between 1.8 Ga and 1.55 Ga, reworked by arc magmatism at 1.3-1.01 Ga and metamorphosed during the assembly of Rodinia at ~0.99 Ga (e.g. Ibañez-Mejia et al., 2011 and references therein).

2.1. Mérida Andes

The basement of the Mérida Andes consists of metasedimentary gneisses, schists and phyllites, and orthogneisses of the Iglesias Complex (Figs. 2, 4; Gonzales de Juana et al., 1980), whose protoliths include ~1 Ga old granitoids and late Cambrian metasedimentary rocks (Van der Lelij et al., 2016b), and was intruded by numerous granitoids that crystallised during ~499 – ~211 Ma. Early Palaeozoic magmatism in the Mérida Andes spans ca. 499 – 415 Ma (Fig. 4; zircon U-Pb ages; Van der Lelij et al., 2016b), and is interpreted to relate to a continental active margin along the north-western corner of Gondwana. The Iglesias Complex records Barrovian, amphibolite facies metamorphism (Grauch, 1972) during crustal thickening at ca. 473 Ma (Van der Lelij et al., 2016b). Post-orogenic extension is recorded by volcanogenic massive sulphides hosted in low grade metasedimentary rocks, which are inter-fingered with volcanic tuffs that yield a zircon U-Pb age of

452.6±2.7 Ma, (Van der Lelij et al., 2016b), and are likely to have formed in a marine basin overlying the Iglesias Complex. Late Palaeozoic to Triassic granitoids and rhyolites in the Paraguana Peninsula, the Serranía del Perijá, Toas Island and the Mérida Andes (Fig. 1, Fig. 4) spanning ~272 – 202 Ma (zircon U-Pb ages, Van der Lelij et al., 2016b), may also be associated with active margin magmatism. Apatite U-Pb and $^{40}Ar/^{39}Ar$ data (van der Lelij et al., 2016a) suggest that rapid cooling of rocks of the Merida Andes at ~250 Ma was driven by exhumation due to increased coupling at the slab-trench interface (Weber et al., 2007; van der Lelij et al., 2016a), although this period of cooling is not recognised in the Santander Massif, possibly due to thermal overprinting during Jurassic magmatism.

There are no published Sm-Nd or Lu-Hf isotopic data from the Mérida Andes. Pb isotopic data suggest that Phanerozoic gneisses and granitoids of the Mérida Andes are autochthonous to the north-western margin of Gondwana (Van der Lelij et al., 2016b), and do not support earlier tectonic models which propose that the north-western corner of Gondwana was amalgamated from numerous allochthonous terranes (Bellizzia and Pimentel, 1994; Aleman and Ramos, 2000). Granitic gneisses from the Iglesias Complex yield a 6 point Rb/Sr isochron age of 440±40 Ma, with an enriched initial $^{87}Sr/^{86}Sr_i$ ratio of 0.708±0.0115 (Kovach et al., 1977), relative to $^{87}Sr/^{86}Sr$ bulk earth values of ca. 0.705 (Allègre et al., 1983). These compositions indicate that these gneisses were partially derived from older components, although they are insufficient to determine the age and nature of the source.

2.2. Santander Massif

The basement of the Santander Massif is mainly composed of gneisses and schists with minor marble, which are intruded by numerous granitoids (Fig. 3; Ward et al., 1974). One published K-Ar date of 945±40 Ma (Goldsmith et al., 1971), and discordant U-Pb data (Restrepo-Pace and Cediel, 2010) tentatively suggest that parts of the basement of the Santander Massif may have formed at ~1 Ga, although all published $^{40}Ar/^{39}Ar$ data from presumed Precambrian units indicate partial to total thermal resetting of the K-Ar system in the Palaeozoic and Jurassic (Restrepo-Pace,

1995; Cordani et al., 2005; van der Lelij et al., 2016a). The metamorphic basement experienced upper amphibolite facies conditions at medium pressures following clockwise pressure-temperature paths, suggesting that barrovian metamorphism was a consequence of crustal thickening (e.g. Ríos et al., 2003; García et al., 2005; Castellanos et al., 2008; Urueña-Suárez and Zuluaga, 2011). Synkinematic magmatic rocks and migmatites record peak metamorphism at ca. 477 Ma (zircon U-Pb; Restrepo-Pace and Cediel, 2010; van der Lelij et al., 2016b). Rocks which record Ordovician barrovian metamorphism were locally overprinted by a second, lower grade metamorphic episode during the Silurian (Castellanos and Ríos, 2015; Mantilla-Figueroa et al., 2016). Early Palaeozoic granitoids intruding the metamorphic basement of the Santander Massif yield zircon U-Pb ages between ~483 and ~439 Ma, and may have formed in a continental active margin (Van der Lelij et al., 2016b). Late Palaeozoic magmatic rocks have not been identified in the Santander Massif, and Early Triassic magmatism is recorded by a rhyolitic dike which intruded sedimentary rocks to the west of the Santa Marta – Bucaramanga Fault at 250.7±4.3 Ma (10VDL58; Fig. 3). Late Triassic magmatism in the Santander Massif is recorded by migmatites and pegmatites which intruded at ~209 Ma (10VDL39, 10VDL43; Fig. 3), and numerous shallow granitoids with ages spanning ca. 206 - 195 Ma (Fig. 3, Fig. 4), which may have also formed along an active continental margin (Spikings et al., 2015; Van der Lelij et al., 2016b). No Precambrian rocks were sampled during this study, although a ~200 Ma diorite, which hosts numerous mafic enclaves, yields a coeval group of concordant zircon U-Pb analyses with a weighted mean age of 1018.3±8.9 Ma (10VDL61; Fig. 3).

Previous isotopic data from the Santander Massif were dominated by Sm-Nd analyses.neisses from the Bucaramanga Gneiss yield $\varepsilon Nd_{945\ Ma}$ values of -4 and -0.5, corresponding to depleted mantle model ages of 1.71 and 1.76 Ga (Ordóñez-Carmona et al., 2006), and two other gneisses from this unit yield $\varepsilon Nd_{1140\ Ma}$ values of -2.6 and -1.1, corresponding to depleted mantle model ages of 1.89 and 1.78 Ga (Cordani et al., 2005). Four samples from the Ocaña Batholith yield $\varepsilon Nd_{413\ Ma}$ values of -3.17 to -2.23, which correspond to model ages of 1.21-1.28 Ga (Ordóñez-Carmona et al., 2006). The Sm-Nd isotopic data from the Ocaña Batholith were calculated on the basis of a hornblende K/Ar age of 413 Ma (Goldsmith et al., 1971), obtained from gneisses in the

area of the intrusion. Recalculated, two stage Sm-Nd model ages (Liew and Hofmann, 1988) for a crystallisation age of ~196 Ma of the Ocaña Batholith (10VDL54; Fig. 3; Van der Lelij et al., 2016b) lie between 1.27 and 1.35 Ga.

Lu-Hf isotopic data have previously been obtained from zircons from one metagabbro in the Santander Massif, which yields a zircon U-Pb age of 477±2 Ma and a weighted mean εHf_t value of 2±1 (Mantilla-Figueroa et al., 2012).

Published whole rock Pb isotopic data from Phanerozoic granitoids exposed in the Santander Massif ($^{207}Pb/^{204}Pb$=15.68-15.79; $^{206}Pb/^{204}Pb$=19.01-20.17; Van der Lelij et al., 2016b) are very similar to Pb-isotopic data acquired from rocks exposed in the Mérida Andes and the north-western Amazonian Craton. These data suggest that these rocks formed in a similar setting, on the north-western margin of Gondwana (Van der Lelij et al., 2016b)

3. Analytical methods

3.1. Zircon Lu-Hf isotopic analyses

Lu-Hf isotopic analyses were performed at the Goethe University of Frankfurt on zircons extracted from 52 igneous and metamorphic rocks from the Mérida Andes and the Santander Massif. Only zircons which previously yielded U-Pb dates corresponding to a magmatic or metamorphic event were selected for analysis, and zircon grains interpreted to record sedimentary protolith ages were ignored. The same zircon domains which were previously analysed for U-Pb geochronology (Van der Lelij et al., 2016b) were ablated using an ASI RESOlution M50 193nm ArF excimer laser. Laser ablation was performed with a spot size of 40 μm for 39 s, using a repetition rate of 5.5 Hz and an on-sample laser energy density of 6 J/cm^2. The ablated material was analysed using a Thermo Scientific Neptune Multicollector Inductively Coupled Plasma Mass Spectrometer (MC-ICP-MS). Time resolved signals were monitored for accidental analysis of multiple zircon domains, and those data were discarded. Isobaric interferences of ^{176}Yb and ^{176}Lu were corrected by monitoring the beam intensities of ^{172}Yb, ^{173}Yb and ^{175}Lu, using the ratios

$^{176}Yb/^{173}Yb$=0.796218 (Chu et al., 2002) and $^{176}Lu/^{175}Lu$=0.02658 (Gerdes and Zeh, 2006). Corrections for instrumental mass bias and mass fractionation were made following the method of Gerdes and Zeh (2006) using custom data reduction software written by Dr. A. Gerdes. The accuracy and external reproducibility of the measurements were monitored by regular analyses of standard zircons Plesovice and GJ-1, which yielded mean $^{176}Hf/^{177}Hf$ ratios of 0.282473±0.000019 (2σ; n=26) and 0.282012±0.000024 (2σ; n=32), respectively. These analytical ratios are in agreement with the long-term isotopic analyses of Plešovice zircon ($^{176}Hf/^{177}Hf$ = 0.282478±0.000025; 2σ; n>450) and GJ-1 zircon ($^{176}Hf/^{177}Hf$=0.282010±0.000025; 2σ; n>800) at the MC-ICP-MS laboratory in Frankfurt. The ages used for the determination of initial $^{176}Lu/^{177}Hf$ ratios and εHf_t values were the weighted mean zircon U-Pb ages of a statistically coeval zircon age population (Van der Lelij et al., 2016b), and used CHUR values of $^{176}Lu/^{177}Hf$ and $^{176}Hf/^{177}Hf$ of 0.0336 and 0.282785, respectively (Bouvier et al., 2008). Two stage hafnium model ages were calculated using age-corrected $^{176}Lu/^{177}Hf$ ratios of the analysed zircons, a $^{176}Lu/^{177}Hf$ ratio of 0.0113 for average continental crust, and juvenile crustal $^{176}Lu/^{177}Hf$ and $^{176}Hf/^{177}Hf$ ratios of 0.0384 and 0.28314 (Gerdes and Zeh, 2006 and references therein).

3.2. Whole rock Sr and Nd isotopic analyses

Sr and Nd isotopic compositions were determined from whole rock powders of 35 fresh igneous and metamorphic rocks, which did not exhibit any alteration in thin section. Approximately 100 mg of whole rock powder was dissolved in 4 ml of concentrated HF and 1 ml of 15M HNO_3 in closed Teflon vials at 140 °C, for seven days. The samples were subsequently dried by evaporation and re-dissolved in 3 ml of 15M HNO_3 before being dried again. Nd and Sr were separated from the matrix using column chemistry following the methods outlined in Pin et al. (1997) and Chiaradia et al. (2011). Nd and Sr isotopic ratios were determined using either a Thermo Scientific Triton Thermal Ionization Mass Spectrometer or a Thermo Scientific Neptune MC-ICP-MS at the University of Geneva, Switzerland. The average analytical uncertainty of measured $^{87}Sr/^{86}Sr$ ratios was 1.2 ppm (2σ), and the accuracy of the interpretation of the reported Sr isotopic compositions is limited mainly by the high potential for fluid-assisted Rb and Sr mobilisation, which can not be

quantified with the available data. Analytical uncertainties of the $^{144}Nd/^{143}Nd$ ratios were propagated into the calculated εNd values. Age corrected isotopic compositions were calculated using Rb/Sr and Sm/Nd ratios determined by trace element analyses and U-Pb ages previously reported by Van der Lelij et al. (2015). Nd model ages (TDM_{Nd}) were calculated using a two stage model with a crustal $^{147}Sm/^{144}Nd$ of 0.12, and depleted mantle $^{147}Sm/^{143}Nd$ and $^{143}Nd/^{144}Nd$ of 0.219 and 0.513151, respectively (Liew and Hofmann, 1988).

3.3. Quartz oxygen isotopic analyses

Two mg of pure quartz was hand picked from 11 granitoids from the Mérida Andes. The purity of the quartz fractions was checked by Raman microprobe at the Geneva Museum of Natural History, Switzerland. Oxygen was extracted from quartz using CO_2 laser fluorination and O isotope compositions were analysed using a Finnigan MAT 253 mass spectrometer at the Institute of Mineralogy and Geochemistry, University of Lausanne, Switzerland. $\delta^{18}O$ values were computed relative to Vienna Standard Mean Ocean Water (VSMOW). Analytical uncertainty for all $\delta^{18}O$ values was better than 0.03 ‰.

4. Results

4.1. Zircon Lu-Hf isotopic analyses

Zircons extracted from 52 granitoids and gneisses exposed in the Merida Andes and the Santander Massif yield 55 discrete zircon U-Pb age populations, each consisting of at least 3 coeval, concordant analyses, with ages spanning between 1018.3±8.9 and 195.8±1.5 Ma (Van der Lelij et al., 2016b). Three of these populations were inherited from igneous or metamorphic protoliths (Van der Lelij et al., 2016b). The dated zircons yield 510 interference corrected $^{176}Lu/^{177}Hf$ ratios ranging between 0.00019 and 0.00474 (average $^{176}Lu/^{177}Hf$ = 0.00143; Appendix Table 1), resulting in very low post-crystallisation radiogenic ingrowth of ^{176}Hf. Nevertheless, all $^{176}Hf/^{177}Hf$ ratios were recalculated to the zircon U-Pb crystallisation ages, and the $^{176}Hf/^{177}Hf_t$ ratios range between 0.282195±0.000017 and 0.282698±0.000026 (Appendix Table 1). The calculated εHf_t values of individual spot analyses (Appendix Table 1) range between -10.0±0.6 (t=488 Ma) and +6.0±0.7

(t=439 Ma), and follow similar trends for the Santander Massif and the Mérida Andes (Figs. 5 and 6).

Calculated weighted mean εHf_t values from 55 zircon populations range between -8.61±0.53 and 5.26±0.44, which correspond to Lu-Hf model ages of 1.57 Ga to 0.77 Ga (Table 1). Individual spot analyses on zircons from several U-Pb age populations (08VDL11B, 08VDL23, 08VDL46 and 10VDL58) yield statistically distinguishable εHf_t values, resulting in large uncertainties for the weighted mean εHf_t values (2σ>1.5 εHf_t units). The zircons from these samples have numerous inherited cores (Van der Lelij et al., 2016b), and we hypothesize that the scatter in these data may derive from the accidental sampling of mixed domains during laser ablation for Lu-Hf analyses, although this was not apparent during the analytical routine itself. The mean εHf_t values in these rocks are not considered to be meaningful and they are not interpreted. Two inherited zircon populations with weighted mean U-Pb ages of ~1018 Ma (10VDL61A) and ~1009 Ma (08VDL11A) yield mean εHf_t values of 2.85 and 3.20, respectively, corresponding to model ages of 1.38 and 1.37 Ga (Table 1). Granitoids, migmatites and gneisses with U-Pb zircon age populations between ~499 Ma and ~472 Ma generally yield the most evolved mean zircon εHf_t values (εHf_t<-5.0; TDM_{Hf} >1.4 Ga; Fig. 5; Table 1), although three samples in this age group yield more juvenile εHf_t values (Fig. 5). Zircon age populations that are younger than ~472 Ma typically yield more juvenile mean εHf_t values of -3.79 to +5.26, which correspond to Lu-Hf model ages of 1.28 to 0.77 Ga and appear to define a general trend to more evolved mean εHf_t values between ~461 Ma and ~443 Ma (Fig. 5). The main outliers in this trend are data from rhyolite 08VDL15 (~453 Ma; εHf_t=+4.5; TDM_{Hf}=0.82; Table 1; Fig. 5) and granite 10VDL46 (~439 Ma; εHf_t =5.26; TDM_{Hf}=0.77; Table 1; Fig. 5) which yield the most juvenile εHf_t values measured in this study.

Granitoids and a rhyolite with U-Pb zircon ages of ~272 Ma to ~196 Ma yield a more restricted range of zircon εHf_t values of -6.55 to -2.46 and Lu-Hf model ages of 1.24 to 1 Ga (Table 1; Fig. 6). More juvenile εHf_t values of ca. +1.3 were obtained from two single zircons from rhyolite 10VDL58 (Table 1; Fig. 6), although the only other two zircons from this sample yielded

much more crustal εHf_t values of -1.0 and -1.8, and the weighted mean εHf_t value of 0.0±2.5 for all four zircons from this sample is not statistically meaningful.

4.2. Whole rock Sm/Nd isotopic analyses

Twenty five whole rock samples with zircon U-Pb ages of ~499 Ma to 415 Ma from the Mérida Andes and the Santander Massif yield age corrected εNd_t values ranging between -7.15 and +1.58 (Fig. 5; Table 1). Granitoids with U-Pb crystallisation ages between ~499 and ~472 Ma yield εNd_t values between -3.22 and -7.15, and include the lowest εNd_t values acquired during this study. Granitoids with U-Pb ages of ~472-~452 Ma and ~442-~415 Ma show generally more juvenile compositions (Fig. 5), with the exception of granite 08VDL41 (εNd_t=-5.39). Granitoids with ages of ~452-~442 Ma show a narrow spread of crustal εNd_t values between -1.83 and -4.06. The isotopically most juvenile sample is rhyolite tuff 08VDL15 (εNd_t = 1.58; Table 1; Fig. 5), which is interfingered with sedimentary rocks. Three whole rock samples with U-Pb ages of ~272 Ma to ~225 Ma (Paraguaná Peninsula, Toas Island and the Perijá Andes; Fig. 1) yield εNd_t values between -3.31±0.38 and -2.20±0.10; whereas younger rocks with crystallisation ages of ~213 Ma to ~198 Ma from the Mérida Andes and the Santander Massif yield more scattered εNd_t, values that range from -7.20 to -2.16 (Fig. 6).

Whole rock εNd_t values obtained during this study correlate well with zircon εHf_t (Fig. 7), and granitoids from both Venezuela and Colombia plot between the trends defined by global recycled orogenic sands and the global mantle array (Vervoort and Patchett, 1996; Vervoort et al., 1999).

4.3. Whole rock Rb/Sr isotopic analyses

Thirty two granitoids yield age corrected whole rock $^{87}Sr/^{86}Sr_i$ ratios that range between 0.7050 and 0.7216 (Table 1; Figs. 5, 6). Two additional granitoids (08VDL38; 10VDL44) yield $^{87}Sr/^{86}Sr_i$ ratios of 0.7010-0.7015, which are less radiogenic than depleted mantle ($^{87}Sr/^{86}Sr$=~0.702; Zindler and Hart, 1986), and have high $^{87}Rb/^{86}Sr$ ratios of 9-11.4 (Table 1), which suggests that Sr

in these rocks may have been mobilized during radiogenic ingrowth. We consider these data points to be unreliable and do not include them in our interpretations. Granitoids with zircon U-Pb crystallisation ages of ~499 Ma to ~472 Ma generally yield more radiogenic $^{87}Sr/^{86}Sr_i$ ratios than rocks with crystallisation ages of ~472 Ma - ~450 Ma (Table 1, Fig. 5). Granitoids which formed between ~450 Ma and ~440 Ma show increasingly radiogenic $^{87}Sr/^{86}Sr_i$ ratios with time. Granitoids from north-western Venezuela (the Paraguaná Peninsula, Toas Island and the Périja Andes; Fig.1), which formed between ~272 Ma and ~225 Ma, yield juvenile $^{87}Sr/^{86}Sr_i$ ratios of ~0.705 (Fig. 6), whereas Triassic to Jurassic rocks with crystallisation ages of ~213 Ma to ~198 Ma from the Mérida Andes and the Santander Massif yield more radiogenic $^{87}Sr/^{86}Sr_i$ ratios.

4.4. Quartz O isotopic analysis

Quartz extracted from 11 granitoids yields $\delta^{18}O$ values ranging between 9.03 and 14.27 ‰ (Table 1; Figs. 5, 6). The highest values of 13.51 ‰ and 14.27 ‰ were obtained from rocks yielding zircon U-Pb ages of ~467 Ma and ~455 Ma (Fig. 5), whereas rocks which formed at 473 Ma and 434 Ma yield the lowest $\delta^{18}O$ values of 9.03 ‰ and 9.56 ‰, respectively.

5.0. Discussion

5.1 The significance of the Lu-Hf model ages

New crust formed by partial melting of depleted mantle has lower $^{176}Lu/^{177}Hf$ ratios than the depleted mantle and the Chondritic Uniform Reservoir (CHUR; e.g. Gerdes and Zeh, 2006 and references therein). As a result, the εHf_t value of any given portion of crust will evolve over time along the crustal evolution trend (Fig. 5), whose slope depends on the $^{176}Lu/^{177}Hf$ ratio of that crust. Consequently, the εHf_t values of crustal rocks which crystallised at different times are not directly comparable. This difficulty is somewhat overcome by interpreting Lu-Hf model ages. The interpretation of crustal evolution trends and model ages relies on the assumption that the continental crust has a known $^{176}Lu/^{177}Hf$ ratio, and remains unchanged by crustal and supracrustal processes (e.g. Hawkesworth and Kemp, 2006). This assumption is invalidated if garnet is fractionated in the melt, because garnet has very different partition coefficients for Lu and Hf and

will decouple the Lu-Hf system from the Sm-Nd system (D_{Lu}/D_{Hf} =~30; Vervoort and Patchett, 1996). Rocks sampled during this study show strong correlations between the Lu-Hf and Sm-Nd systems (Fig. 7), suggesting that garnet fractionation was not an important process in the melt source. Melts which form in continental active margins may derive from igneous, sedimentary or mixed sources (e.g. Dalziel, 1986; Collins and Richards, 2008), and Lu-Hf model ages may approximate the average age of extraction from depleted mantle of the various components in the melt source, unless a homogeneous source can be determined by other means (Hawkesworth and Kemp, 2006).

Lu-Hf model ages calculated from our data range between 0.77 Ga and 1.57 Ga, and are 0.04 Ga to 0.36 Ga (average 0.2 Ga) younger than the Sm-Nd model ages from the same rocks (Table 1). This discrepancy may arise because either the crustal $^{176}Lu/^{177}Hf$ ratio of 0.0113 (Gerdes and Zeh, 2006) or the crustal $^{147}Sm/^{144}Nd$ ratio of 0.12 (Liew and Hofmann, 1988) may not be representative of the average crustal end members for granitoids in this study. Existing whole rock data from Precambrian gneisses in Colombia indicate varying $^{147}Sm/^{144}Nd$ ratios that range from 0.0686 to 0.1904 (Cordani et al., 2005; Ordóñez-Carmona et al., 2006; Ibañez-Mejia et al., 2015), and therefore the $^{147}Sm/^{144}Nd$ ratio of ~0.12 used for our calculations appears to be a reasonable assumption. Alternatively, in mixed source magmas the Lu-Hf system may be more sensitive to melt additions from depleted mantle derived sources than the Sm-Nd system, because of their respective concentrations (Hf_{MORB}/Hf_{Crust} = ~0.54, Nd_{MORB}/Nd_{Crust} = ~0.35; Rollinson, 1993). Therefore, we prefer to consider the Lu-Hf model ages as a minimum estimate of the average time when the various source components were extracted from the depleted mantle.

5.2. Isotopic correlations

Although Strontium isotopic compositions are susceptible to modification by fluid flow or alteration, initial $^{87}Sr/^{86}Sr_i$ ratios correlate with Lu-Hf model ages, $\delta^{18}O$ values and the alumina saturation index (A/CNK or Shand's Index, e.g. Maniar and Piccoli, 1989) for most granitoids in the study area (Fig. 8) suggesting that, as a whole, the analysed Sr isotopic compositions reflect the

compositions of the granitoids during crystallisation. The correlation between $^{87}Sr/^{86}Sr_i$ ratios and Lu-Hf model ages suggests that melt components from granitoids in the study area were derived from a combination of older felsic, and younger mafic sources. The two Mesozoic samples from the Santander Massif are outliers in this trend (Fig. 8): one is a migmatite (10VDL43B) and the other is from a rock with numerous enclaves (10VDL61B), both of which may have mixed $^{87}Sr/^{86}Sr$ compositions which cannot be adequately time corrected. The correlation of $^{87}Sr/^{86}Sr_i$ with $\delta^{18}O$ values and A/CNK (Fig. 8) suggests that felsic, Rb rich endmembers included pelites and likely were metasedimentary rocks (e.g. Chappell and White, 1974; Harris et al., 1997). Rocks with the lowest $^{87}Sr/^{86}Sr_i$ ratios of <0.706 exhibit a range of Lu-Hf model ages (Fig. 8). Hence, if we assume that Sr was not remobilized for these samples, mafic endmembers may be heterogeneous in age, and may include partially rejuvenated, mafic lower crust which originally formed at ~1.6 Ga (e.g. Ibañez-Mejia et al., 2011, 2015). These data also suggest that these granitoids are not amenable to a clear-cut classification by melt source with geochemical discriminators (with S-Type granite having A/CNK > 1.1, e.g. Chappell and White, 1974; Maniar and Piccoli, 1989) or isotopic discriminators (with S-Type granite yielding quartz δ18O > 12‰, e.g. Harris et al., 1997) because many of the sampled lithologies appear to be the product of mixes of melt derived from several source types.

As the Lu-Hf and Sm-Nd isotopic systems both record the timing of melt depletion from a depleted mantle source and correlate very well (Fig. 7), our discussion focuses more around the Lu-Hf isotopic system for mantle melt contributions because Lu-Hf data were obtained from more samples.

5.3. Precambrian Basement

The isotopic composition of Precambrian basement was only determined indirectly by Lu-Hf analysis of inherited zircon populations with U-Pb ages of ~1.01 Ga, obtained from an orthogneiss from the Mérida Andes and xenoliths in the Santander Massif. These zircons populations yield Lu-Hf model ages of ~1.37 Ga (Table 1), which are compatible with previous suggestions that ~1.01 Ga rocks located along north-western Amazonia were formed in a juvenile

arc with variable contamination by sources that were older than 1.55 Ga (Ibañez-Mejia et al., 2011; Weber et al., 2010).

5.4. 499 Ma – 472 Ma

The Early Palaeozoic orogenesis is recorded in the Santander Massif and the Mérida Andes by upper amphibolite facies Barrovian metamorphism (Fig. 4; Grauch, 1972; García et al., 2005; Castellanos et al., 2008; Urueña-Suárez and Zuluaga, 2011), which affected all rocks older than ~472 Ma (Van der Lelij et al., 2016b). Peak metamorphism resulted in anatexis of the continental crust at ~477.0±5.3 Ma (migmatite 10VDL50; Van der Lelij et al., 2016b) and the intrusion of strongly foliated, synkinematic granitoids between ~489 Ma and ~472 Ma (Ward et al., 1974; Kovach et al., 1977; Restrepo-Pace and Cediel, 2010; van der Lelij et al., 2016b). Barrovian metamorphism is typical of orogenesis driven by crustal thickening (e.g. Spear, 1993), and previous authors have related Early Palaeozoic orogenesis in the Northern Andes to the docking of an allochthonous terrane which encompasses the basement of the Santander Massif (Chibcha Terrane; e.g. Ramos, 2009). Pb isotopic data collected from granitoids and gneisses from both the Mérida Andes and the Santander Massif are consistent with an autochthonous origin (Van der Lelij et al., 2016b), and Nd, Sr, and Hf isotopic trends are similar for rocks from the Santander Massif and the Mérida Andes (Fig. 5, 6), providing further support for a common history on the margin of Gondwana. Orogenesis as a result of continental collision seems unlikely, because palaeomagnetic and faunal data indicate that during the Ordovician, Gondwana was separated from Baltica and Laurentia by the Iapetus and Tornquist Oceans, respectively (e.g. Cocks and Torsvik, 2002). Instead, we propose that Ordovician orogenesis in the Mérida Andes and the Santander Massif was driven by increased plate coupling between subducting oceanic lithosphere of the Iapetus Ocean and the overriding margin of Gondwana (Fig. 9A; Dalziel, 1986; Gutscher, 2002), in a similar setting to Early Palaeozoic orogenic belts elsewhere along the margin of Gondwana (e.g. Collins, 2002; Lucassen and Franz, 2005; Kemp et al., 2009).

Most of the rocks which crystallised between ~499 and ~472 Ma yield (Fig. 5) i) zircon εHf_t values which include the most negative values obtained during this study of ~-7, corresponding

to the oldest model ages of ~1.4 - ~1.6 Ga, ii) the most negative whole rock εNd_t values of ~-4 to ~-7, iii) strongly radiogenic whole rock $^{87}Sr/^{86}Sr_i$ ratios of 0.710-0.713 suggesting evolved, Rb rich sources, and iv) quartz $\delta^{18}O$ values <12 ‰, which suggests derivation from igneous sources (Table 1; Fig. 5; Harris et al., 1997). These data suggest that the magmatic sources were evolved and may include middle to upper continental crust, rather than lower crustal or mantle derived rocks. Migmatite 10VDL50 is hosted in a paragneiss (Van der Lelij et al., 2016b), suggesting that its ~1.2 Ga Lu-Hf model age represents the average model age of the sedimentary components in the protolith, which was derived from a mix of ~1 Ga and older continental crust.

5.5. 472 Ma - 452 Ma

Numerous active margin granitoids with zircon U-Pb ages younger than ~472 Ma crosscut the foliation of the metamorphic basement in the Mérida Andes and the Santander Massif, and are interpreted to post-date peak metamorphic conditions (Fig. 4; Restrepo-Pace and Cediel, 2010; van der Lelij et al., 2016b). In the Mérida Andes, interfingered marine sedimentary rocks (Mucuchachi Fm.; Fig. 2) and volcanic tuffs (Las Tapias rhyolite 08VDL15; 452.6±2.7 Ma; Fig. 4; Table 1) unconformably overlie the upper amphibolite facies metamorphic basement (Fig. 4), and host volcanogenic massive sulphides (Staargaard and Carlson, 2000). Non metamorphosed, Late Ordovician graptolite bearing sandy siltstones and sandstones of the Caparo Fm. also overlie basement rocks in the southern flank of the Mérida Andes (Fig. 4; Odremán and Useche, 1997). These relationships suggest that upper amphibolite facies gneisses which metamorphosed during orogenesis and crustal thickening between ~499 and ~472 Ma, were unconformably overlain at ~453 Ma by marine basins. Therefore, in this time frame, the orogeny must have subsided either by post-orogenic collapse or intra-arc or back-arc extension. Even though the variations of crustal thickness of north-western Gondwana during the Palaeozoic cannot be quantitatively assessed using any published data, i) continuous magmatism in the Mérida Andes and the Santander Massif between ~499 and ~415 Ma, ii) the formation of marine basins at ~453 Ma over ~499-~472 Ma amphibolite facies metamorphic basement requiring exhumation from at least ~8km during extension, and iii) the VMS mineralisation of the marine sediments of the Muchuchachi Fm. (e.g.

Staargaard and Carlson, 2000) are consistent with an intra-arc or back arc basin setting at ~453 Ma (Fig. 8; e.g. Schandl and Gorton, 2002).

Granitoids which formed between ~472 and ~453 Ma in the Mérida Andes and the Santander Massif generally yield (Fig. 5; Table 1) i) Lu-Hf model ages of ~1.0 to ~1.2 Ga; ii) εNd_t values of ~-4 to ~+2; iii) $^{87}Sr/^{86}Sr_i$ ratios of 0.705 to 0.708 suggesting mafic sources with low Rb concentration. Biotite granite 08VDL41 (454.5±3.1 Ma; Table 1) is an outlier in terms of isotopic composition in this age range, yielding an $^{87}Sr/^{86}Sr_i$ ratio of 0.7137 and a quartz $\delta^{18}O$ of 14.27 ‰, suggesting that it has a sedimentary protolith (S-type granite; Harris et al., 1997). The Lu-Hf model age of this rock is the oldest of this age group (1.21 Ga; Table 1), indicating that the sedimentary protolith may have mixed components of ~1.0 Ga and older crust, both of which may be found in the basement near the Northern Andes (Ibañez-Mejia et al., 2011; Baquero et al., 2015). The quartz O isotopic data from granodiorite 08VDL44 ($\delta^{18}O$=13.51; 466.8±2.5 Ma; Table 1; Fig. 5) are also typical for S-Type granite (Harris et al., 1997), although its low $^{87}Sr/^{86}Sr_i$ ratio of 0.7076 is indicative of a low average Rb/Sr ratio source rock, which is more suggestive of the lower crust (e.g. Rudnick and Fountain, 1995). These data suggest that this rock was derived from mixed sources between a mafic lower crustal or mantle end-member and sedimentary sources.

The isotopic data suggest that most of the granitoids which formed between ~472 and ~452 Ma derived from mafic sources with low Rb/Sr ratios, such as i) ~1.0-1.2 Ga lower crust (Fig. 9), ii) a mixture between depleted mantle sources and older crustal sources, or iii) enriched mantle sources such as sub-continental lithospheric mantle. Our data cannot discriminate between these scenarios and the only rock from this age group which is sufficiently isotopically juvenile to require a melt contribution from depleted mantle is rhyolite 08VDL15, whose Lu-Hf model age of 0.8 Ga (Table 1) cannot be accounted for by derivation from mixes of ~1 Ga and older crust.

The Micarache Orthogneiss (08VDL11; Figs 2, 7) has two zircon populations with U-Pb ages of 1008.6±6.7 Ma and 454.0±10 Ma, which yield different Lu-Hf model ages of ~1.37 Ga

and ~0.95 Ga, respectively (Table 1). This unfoliated, biotite rich rock exhibits lobate grain boundaries and myrmekite, sillimanite replaced by muscovite, biotite and myrmekite symplectites (Van der Lelij et al., 2016b), and ~50 μm grains of partially resorbed, anhedral orthopyroxene, which suggests the protolith was a granulite facies rock (Spear et al., 1999). The microtextural and geochronological data suggests that this rock had a ~1009 Ma protolith which underwent anatexis at ~454 Ma (Van der Lelij et al., 2016b). A simplistic interpretation of the Lu-Hf data may suggest that juvenile material was added to the rock at ~454 Ma, although this is inconsistent with microtextural evidence indicating that this rock may have been a closed system with regards to melt. Granulite facies textures suggest that biotite may have been unstable or absent and garnet may have been present in the protolith (Spear et al., 1999). The high Lu/Hf ratio of garnet may have resulted in more ingrowth of radiogenic Hf in garnet by ~454 Ma than the bulk rock. Biotite can form by hydration breakdown of garnet during high temperature retrograde reactions (Spear et al., 1999), and we hypothesize that rehydration of the granulite facies protolith resulted in retrograde reactions of garnet to biotite and partial anatexis of the rock at ~454 Ma. This process would have resulted in the crystallisation of zircons at isotopic disequilibrium with the bulk rock Hf composition, and is consistent with isotopic, geochronologic and microtextural evidence.

5.6. 452 Ma - 442 Ma

Geochemical arguments suggest that granitoids with zircon U-Pb crystallisation ages of ~452 Ma to ~442 Ma formed during continuing arc magmatism (van der Lelij et al., 2016b). Sedimentary rocks from this period are sparse in the Northern Andes, and a hiatus spanning ~10 Ma is recorded in the Mérida Andes (Fig. 4) between the Caparo Formation (Sandbian; ~461 Ma - ~456 Ma; Gonzales de Juana et al., 1980) and the El Horno Fm. (LLandovery - Early Wenlock; 444 Ma - 426 Ma; Gonzales de Juana et al., 1980). The duration of sedimentation within the basins which host the volcano-sedimentary Mucuchachi Fm. (~453 Ma; Table 1) in the central Mérida Andes is unknown.

Granitoids which formed between ~452 Ma and ~442 Ma yield increasing Lu-Hf model ages, more negative εNd_t values and increasing $^{87}Sr/^{86}Sr_i$ ratios with time (Fig. 5), suggesting increasing contributions of old, middle to upper crust. The quartz $\delta^{18}O$ values of 11.30 and 12.07 obtained from two granitoids (Table 1; Fig. 5) suggest that they received melt contributions from sedimentary sources (Harris et al., 1997). The isotopic trends contrast sharply with trends recorded during the preceding period of extension. Combined with the apparent hiatus in the Northern Andes (Fig. 4) and evidence for metamorphic overprints of Silurian age in parts of the Santander Massif (Mantilla-Figueroa et al., 2016), we propose that the increasingly crustal isotopic signal recorded during this period reflects basin inversion and the development of positive relief (Fig. 9). Compression during this period may have resulted in tectonic burial of metasedimentary rocks of the middle to upper crust, which were previously too shallow to melt.

5.7. 443 Ma - 415 Ma

Only three granitoids from the Santander Massif and the Mérida Andes yield zircon U-Pb ages ranging between ~439.2 Ma and 414.5 Ma (Table 1). The Lu-Hf model age of granite 10VDL46 (439.2±4.7 Ma; T_{NC}=0.77 Ga; Table 1) is the youngest recorded in Palaeozoic rocks of the Santander Massif and the Mérida Andes, and requires a juvenile input from a depleted mantle. Granite 10VDL46 was altered by numerous crosscutting quartz veins, and as a consequence no attempts were made to extract additional isotopic data from this rock. Sedimentary basins which formed coevally with granite 10VDL46 exist in the Mérida Andes (El Horno Fm.; see above), and although these data are consistent with an extensional regime favorable to the intrusion of melt derived from the depleted mantle, further evidence is necessary to corroborate this interpretation. The two other granitoids from this age group yield Lu-Hf model ages that increase with younger crystallisation ages, decreasing εNd_t values, increasing $^{87}Sr/^{86}Sr_i$ ratios and increasing quartz $\delta^{18}O$ values, suggesting increasing crustal contributions between ~434 Ma and ~415 Ma. Sedimentation is recorded in the Mérida Andes until the Early Wenlock (~426 Ma, Fig. 4), which was followed by a regional sedimentary hiatus until the middle Devonian (~398 Ma; Van der Lelij et al., 2016b), and field relationships and data are too sparse to constrain the tectonic environment.

5.8. ~272 Ma – ~196 Ma

Whole rock geochemistry is consistent with a continental arc setting for granitoids and rhyolites that crystallised during ~272 Ma to ~196 Ma (Van der Lelij et al., 2016b). Three granitoids were collected from isolated basement exposures in the Paraguaná peninsula, the foothills of the Perijá range and Toas Island in north-western Venezuela (Fig. 1). These rocks yield similar Lu-Hf model ages of 1.08 Ga to 1.2 Ga, εNd_t values of -2.2 to -3.31 with Sm-Nd model ages of 1.17 Ga to 1.24 Ga, and $^{87}Sr/^{86}Sr_i$ ratios of 0.705 to 0.7053 (Table 1; Fig. 6). The isotopic data suggest that Rb-poor, lower crustal sources were involved in the petrogenesis of these granitoids. Basement rocks extracted from drill cores beneath Lake Maracaibo and the Falcón Basin, and from an inlier in Guajira Peninsula (Fig. 1) yield zircon U-Pb crystallisation ages of ~1 Ga and Sm-Nd model ages of 1.2 to 1.3 Ga (Baquero et al., 2011, 2015), and may represent a plausible melt source for granitoids in north-western Venezuela.

Fifteen granitoids, two felsic volcanic rocks, one pegmatite and one migmatite from the Mérida Andes and the Santander Massif with zircon U-Pb ages ranging between ~251 and ~196 Ma yield Lu-Hf model ages of 0.91 Ga to 1.24 Ga, and no time-related trends are observed (Fig. 6; Table 1). The most juvenile Hf isotopic composition with an average Lu-Hf model age of 0.91 Ga is from a rhyolite dike in the Santander Massif, which intruded the Bocas Fm. at ~251 Ma (10VDL58; Fig. 6; Table 1), and may include melt from a depleted mantle end member, although the individual analyses from this sample are not statistically equivalent and define a large spread. The exhumation episode recognised in the Merida Andes at ~250 Ma from thermochronological data (van der Lelij et al., 2016a) which was presumably driven by regional compression (Weber et al., 2007) did not have a clear effect on the isotopic signature of rhyolite 10VDL58, which is the only coeval magmatic rock. However, exhumation at ~250 Ma is not recorded in the Santander Massif (van der Lelij et al., 2016a). Similarly, extension between ~240 and ~215 Ma recorded in the Central Cordillera of Colombia and Eastern Cordillera of Ecuador by field and isotopic data (Cochrane et al., 2014a) are not recorded in the Merida Andes and Santander Massif due to a paucity of coeval

sedimentary rocks and absence of clear isotopic trends. This emphasises variability in crustal response and magmatic processes across the same margin.

Igneous rocks from the Mérida Andes and the Santander Massif, which formed between ~213 Ma and ~196 Ma, yield radiogenic $^{87}Sr/^{86}Sr_i$ ratios of 0.708 to 0.7216 (Fig. 6; Table 1), suggesting that some melt was derived from Rb-rich end-members, which may include middle to upper crustal rocks and sedimentary protoliths. Extension at ~200 Ma in the Mérida Andes and the Santander Massif resulted in deposition of graben-filling sandstones of the La Quinta and Jordan formations (Kammer and Sánchez, 2006; van der Lelij et al., 2016b), and the eruption of pillow basalts between the late Triassic and ~185 Ma in the eastern Cordillera (Moreno-Sánchez et al., 2016). However, this does not seem to have resulted in more primitive isotopic compositions of late Triassic to Early Jurassic granitoids sampled during this study, suggesting that extension until ~196 Ma may have been insufficient to facilitate intrusion of depleted mantle melts into the upper crust in the studied area. Extension driven by slab roll-back resulted in the arc axis migrating westward into the Central Cordillera of Colombia by ~190 Ma (Cochrane et al., 2014b; Spikings et al., 2015), where isotopic signatures define a clear trend towards more juvenile melt sources and increasing mantle contribution with time, until ~145 Ma (Cochrane et al., 2014b).

6. Melt sources, heat advection and crustal recycling

Although it is generally agreed that some granitoids derive from the melting of sedimentary protoliths (S-Type granites; e.g. Chappell and White, 1974; Harris et al., 1997), there is considerable controversy about the sources of I-Type granites. Some authors suggest that I-Type granites form by melting of calc-alkaline crustal rocks of mafic to intermediate composition without any direct mantle contribution (e.g. Roberts and Clemens, 1993; Clemens et al., 2011), although others consider that mantle-derived melts may be the dominant component (e.g. Pitcher, 1997; Annen et al., 2008; Nandedkar et al., 2012).

Phanerozoic granitoids from the Mérida Andes and Santander Massif are difficult to classify utilising the I-Type and S-Type scheme according to their major element compositions (Van der Lelij et al., 2016b). For example, while the mainly peraluminous geochemistry of the granitoids suggests that they may include S-Type granites (e.g. Chappell and White, 1974), many of these granitoids yield Na_2O/K_2O ratios typical of I-Type granite (e.g. Chappell and White, 1974; van der Lelij et al., 2016b). The isotopic data presented here suggests that both I-Type and S-Type granites may have formed coevally, and that some granitoids are hybrids. For example, granite 08VDL41 has quartz $\delta^{18}O$ and $^{87}Sr/^{86}Sr_i$ compositions typical of S-Type granite (Table 1), whereas coeval rocks from the same regions which intruded at ~454 Ma yield juvenile $^{87}Sr/^{86}Sr_i$ compositions suggesting a much less evolved source, although the Lu-Hf model ages of these rocks all fall in the same ~1.0 Ga to ~1.2 Ga range (Table 1; Fig. 5). Regardless of whether the source included igneous or sedimentary protoliths, the isotopic data suggest that the average mixed source age was between ~1.0 Ga to ~1.6 Ga for most rocks in the Merida Andes and the Santander Massif.

The change of Lu-Hf model ages from mainly ~1.4-~1.6 Ga to mainly ~1.0-~1.2 Ga after ~472 Ma suggests that a change of average melt source was coeval with the cessation of metamorphism, and may relate to post-orogenic extension or back-arc or intra-arc basin opening (Fig. 9). Crustal end-members of both 1.4-1.6 Ga and 1.0-1.2 Ga may have been present outboard of the Amazonian craton at ~1 Ga (Ibañez-Mejia et al., 2011; Weber et al., 2010), and the shift in isotopic trends at ~472 Ma suggests that extension between ~472 Ma and ~452 Ma resulted in sufficient heating and decompression of the lower, more juvenile crust to generate melt (Fig. 9). Granitoids which intruded between ~472 Ma and ~196 Ma show only restricted variations of average zircon Lu-Hf model ages which lie mainly between 1.0 and 1.2 Ga (Figs. 5,6), however they exhibit large variations of $^{87}Sr/^{86}Sr_i$ suggesting that they were derived from both lower and upper crustal sources. The structural dissection during extension between ~472 and ~452 Ma may gave juxtaposed upper crustal lithologies with more mafic lithologies, effectively mixing them together. Therefore, the ~472 Ma shift to more juvenile Hf compositions may reflect a homogenisation of source reservoirs for magmatic rocks in the Mérida Andes and the Santander

Massif, and these source reservoirs subsequently evolved along normal crustal evolution trends (Figs. 5, 6) without significant juvenile input until ~196 Ma. Only two Early Palaeozoic granitoids (08VDL55, 10VDL46; Table 1, Fig. 5) and two rhyolites (08VDL15; 10VDL58; Table 1, Figs. 5, 6) in the Mérida Andes and the Santander Massif yield Lu-Hf model ages of < 1.0 Ga, which cannot be accounted for by derivation from local crustal end-members. However, these samples represent only a minor proportion percent of our total dataset, and we consider that they represent only minor contributions of depleted mantle derived melt to the crust. These findings are consistent with the conclusions of other studies of the western margin of South America (e.g. Willner et al., 2008; Bahlburg et al., 2009; Mišković and Schaltegger, 2009; Reimann et al., 2010; Dahlquist et al., 2012; Augustsson et al., 2016), which suggest that most Palaeozoic igneous rocks which formed on the western margin of Gondwana mainly recycled Mesoproterozoic to Neoproterozoic crust.

Partial melting of continental crust can occur without mantle melt input, during thermal equilibration of thrust sheets which were juxtaposed by orogenesis or by crustal delamination (e.g. Thompson and Connolly, 1995; Petford et al., 2000). In Early Palaeozoic rocks of the study area, peak temperature conditions during Barrovian metamorphism were reached at ~477-473 Ma, and minimum crustal thickness appears to have been reached at ~453 Ma (Fig 9). Therefore, both of these mechanisms for heating and melting of the crust between ~499 and ~415 Ma may have operated successively. The continental arc setting for the Palaeozoic and Early Jurassic rocks of Venezuela and Colombia (Fig. 9) suggests that dehydration of the subducting slab may have partially melted the mantle wedge, resulting in heat advection to the lower crust by underplating of mafic melts, permitting crustal anatexis and the generation of felsic melts (e.g. Huppert and Sparks, 1988; Petford et al., 2000). This hypothesis predicts that the lower continental crust may have become more juvenile as mafic underplating of mantle derived basalts continued. Trends of increasing juvenile components with time may be observed in Phanerozoic arcs, for example in Australia (e.g. Kemp et al., 2009; Collins et al., 2011) and in the Central Cordillera of Colombia and eastern Cordillera of Ecuador (Cochrane et al., 2014b). In the regions sampled during this study, relatively constant Lu-Hf model ages of ~1.0 Ga to ~1.2 Ga from rocks which formed

between ~472 Ma and ~196 Ma (Fig. 5, 6) suggest that there was no juvenile crust forming in the Merida Andes and the Santander Massif after ~472 Ma. However, crustal growth during extension is clearly documented in the Central Cordillera of Colombia (Fig.1) between ~240 and ~215 Ma (Cochrane et al., 2014a; Spikings et al., 2015), where progressively more juvenile mafic material injected in the crust yields εHf_t values of +10 to +15, precluding any substantial crustal contribution, resulting in Lu-Hf model ages close to the crystallisation age. Consequently, rocks exposed in the Santander Massif and Merida Andes may not have been affected by early Triassic extension, although they were part of the same convergent margin (Spikings et al., 2015).

Recent studies have suggested that mafic, mantle derived melts may delaminate and be recycled in the mantle after transferring heat to the crust (e.g. Arndt and Goldstein, 1989; Jull and Kelemen, 2001; Davidson and Arculus, 2006), resulting in isotopically enriched sub-continental lithospheric mantle (e.g. Willbold and Stracke, 2010). Although there are presently no direct measurements of the isotopic composition of the mantle beneath the north-western margin of Gondwana, the overall absence of definite trends in Lu-Hf model ages between ~472 and ~196 Ma in the Merida Andes and Santander Massif, combined with highly varying $^{87}Sr/^{86}Sr_i$ ratios suggest that any contributed mantle derived material, may have had broadly similar Lu-Hf isotopic compositions to the crust. This is consistent with enrichment of the mantle by crustal recycling processes beneath long-lived arc systems such as the Andes (e.g. Willbold and Stracke, 2010), and consequently crustal growth by melt extraction from the depleted mantle may occur only during more protracted crustal thinning than is recorded in the Mérida Andes and the Santander Massif.

7. Conclusions

A comprehensive isotopic overview of rocks from the Santander Massif and the Mérida Andes shows that:

1. Granitoids from the Mérida Andes, Venezuela and the Santander Massif, Colombia crystallised from melts derived from both igneous and sedimentary sources, which can be identified by combining O, Sr and Lu-Hf isotope analyses.

2. Sources for granitic magmatism can be correlated with independently constrained geodynamic settings. During orogenesis at ~499-~473 Ma, granitic melt was derived from ca. 1.2 Ga and 1.4-1.6 Ga crust (Fig. 9). Possible crustal end member source for this crust include Precambrian basement units which are exposed in the Garzón Massif (Fig. 1) and adjacent regions (Ibañez-Mejia et al., 2011) and sedimentary rocks that host detritus derived from these units.

3. During post-orogenic extension, magmatic sources switched rapidly to more juvenile, lower crustal compositions (Fig. 9). Although the isotopic compositions of two granitoids and two rhyolites require input from the depleted mantle, the overall isotopic composition of post-472 Ma granitoids suggests that their melt derived from the recycling of variable, lower to upper crustal end members with contributions from enriched mantle sources that cannot be quantified using our data.

4. A trend towards slightly older, more Rb rich sources may be recorded in granitoids which formed between ~452 Ma and ~442 Ma. This period was coeval with the development of regional unconformities, suggesting that these rocks formed during a brief period of compression.

5. The relatively minor variations of Lu-Hf model ages compared to $^{87}Sr/^{86}Sr_i$ ratios after 472 Ma suggests that the lower crust may have been only slightly more juvenile than the upper crust. This indicates that sedimentary processes in the upper crust may have reworked ca. 1 Ga middle to lower crust, and that only minor sedimentary input was derived from older sources.

6. Quantitative determination of relative contributions of enriched mantle and crust cannot be made because the Palaeozoic isotopic composition of the mantle below north-western South America is unknown. Direct input from depleted mantle sources may only be recorded in less than 10% of the samples analysed in this study, and a majority of these samples can be related in space and time with basin formation and/or extension in the Mérida Andes.

7. The paucity of absolute trends to more juvenile Lu-Hf model ages after ~472 Ma suggests that the advection of heat by mantle derived melt to the lower crust, which may be a requirement for the generation of granitoids, was compensated either by i) delamination of the juvenile portion of the lower crust subsequently to heat advection, or ii) progressive enrichment of the sub-continental lithospheric mantle composition, or both.

8. There is only minor evidence for crustal growth between ~1 Ga and ~196 Ma in the Mérida Andes and the Santander Massif in spite of evidence for periods of extension of the continental crust.

9. The breakdown of garnet to biotite during partial anatexis of granulite facies rocks can result in the formation of zircons that inherit juvenile Hf compositions in isotopic disequilibrium with the bulk rock.

Acknowledgements

The authors are grateful to Prof. Tabata Hoeger, Daniela Tazzo and Maria Carolina Maninat from ULA Mérida for field assistance in Venezuela, and to Prof. Mauricio Bermúdez for logistical support. Field work and logistics in Colombia were greatly facilitated by the generous assistance of Ecopetrol. Kerstin Bauer from the University of Lausanne kindly performed stable isotope analyses, and Cedric Schnyder from the Natural History Museum of Geneva assisted with Raman microprobe analyses. We thank Luigi Solari for a constructive review and editor Joseph Meert for editorial handling which allowed us to further improve the manuscript. This project was funded by the Swiss National Science Foundation fund 200021_129497, which was awarded to RS.

References

Aleman, A., Ramos, V.A., 2000. The Northern Andes, in: Cordani, U.G., Milani, E.J., Thomaz, A., Campos, D.A. (Eds.), Tectonic Evolution of South America. Presented at the 31st International Geological Congress, Rio de Janeiro, Brazil, pp. 453–480.

Allègre, C.J., Hart, S.R., Minster, J.-F., 1983. Chemical structure and evolution of the mantle and continents determined by inversion of Nd and Sr isotopic data, II. Numerical experiments and discussion. Earth and Planetary Science Letters 66, 191–213.

Amante, C., Eakins, B.W., 2008. ETOPO1 1 arc-minute global relief model: procedures, data sources and analysis. National Geophysical Data Center, NESDIS, NOAA, US Department of Commerce, Boulder, CO.

Annen, C., Blundy, J.D., Sparks, R.S.J., 2008. The sources of granitic melt in Deep Hot Zones. Transactions of the Royal Society of Edinburgh, Earth Sciences 97, 297–309.

Annen, C., Blundy, J.D., Sparks, R.S.J., 2006. The genesis of intermediate and silicic magmas in deep crustal hot zones. Journal of Petrology 47, 505–539.

Armstrong, R.L., 1991. The persistent myth of crustal growth. Australian Journal of Earth Sciences 38, 613–630.

Arndt, N.T., Goldstein, S.L., 1989. An open boundary between lower continental crust and mantle: its role in crust formation and crustal recycling. Tectonophysics 161, 201–212.

Augustsson, C., Münker, C., Bahlburg, H., Fanning, C.M., 2006. Provenance of late Palaeozoic metasediments of the SW South American Gondwana margin: a combined U–Pb and Hf-isotope study of single detrital zircons. Journal of the Geological Society 163, 983–995.

Augustsson, C., Willner, A.P., Rüsing, T., Niemeyer, H., Gerdes, A., Adams, C.J., Miller, H., 2016. The crustal evolution of South America from a zircon Hf- isotope perspective. Terra Nova.

Bahlburg, H., Vervoort, J.D., Du Frane, S.A., Bock, B., Augustsson, C., Reimann, C., 2009. Timing of crust formation and recycling in accretionary orogens: Insights learned from the western margin of South America. Earth-Science Reviews 97, 215–241.

Baquero, M., Grande, S., Urbani, F., Cordani, U., Hall, C., Armstrong, R., 2015. New Evidence for Putumayo Crust in the Basement of the Falcon Basin and Guajira Peninsula, Northwestern Venezuela. AAPG Memoir 108, 105–138.

Baquero, M., Grande, S., Urbani, F., Cordani, U.G., Sato, K., Schaaf, P., Hall, C.M., Mendi, D., Azancot, M., 2011. New LA-ICP-MS U-Pb zircon dating, 40Ar-39Ar and Sm-Nd model ages: Evidence of the Grenvillian Event in the basement of the Falcón and Maracaibo Basins, northwestern Venezuela. Presented at the XIV Congreso Latinoamericano de Geología, Medellin, Colombia.

Bellizzia, A., Pimentel, N., 1994. Terreno Mérida: Un cinturón alóctono herciniano en la Cordillera de Los Andes de Venezuela, in: V Simposio Bolivariano Exploracion Petrolero. Caracas, Venezuela, pp. 271–290.

Bermúdez, M.A., van der Beek, P., Bernet, M., 2011. Asynchronous Miocene-Pliocene exhumation of the central Venezuelan Andes. Geology 39, 139–142.

Boekhout, F., Roberts, N.M., Gerdes, A., Schaltegger, U., 2015. A Hf-isotope perspective on continent formation in the south Peruvian Andes. Geological Society, London, Special Publications 389, 305–321.

Bouvier, A., Vervoort, J.D., Patchett, P.J., 2008. The Lu–Hf and Sm–Nd isotopic composition of CHUR: constraints from unequilibrated chondrites and implications for the bulk composition of terrestrial planets. Earth and Planetary Science Letters 273, 48–57.

Castellanos, O.M., Ríos, C.A., 2015. A case of regional metamorphism of Buchan type (andalusite-cordierite) in the Nortern Santander Massif, Eastern Cordillera (Colombia). Revista de la Academia Colombiana de Ciencias Exactas, Físicas y Naturales 39, 416–429.

Castellanos, Ó.M.A., Ríos R, C.A., Takasu, A., 2008. A new approach on the tectonometamorphic mechanisms associated with PT paths of the Barrovian-type Silgará Formation at the Central Santander Massif, Colombian Andes. Earth Sciences Research Journal 12, 125–155.

Chappell, B.W., White, A.J.R., 1974. Two contrasting granite types. Pacific Geology 8, 173–174.

Chiaradia, M., Müntener, O., Beate, B., 2011. Enriched Basaltic Andesites from Mid-crustal Fractional Crystallization, Recharge, and Assimilation (Pilavo Volcano, Western Cordillera of Ecuador). Journal of Petrology 52, 1107–1141.

Chu, N.-C., Taylor, R.N., Chavagnac, V., Nesbitt, R.W., Boella, R.M., Milton, J.A., German, C.R., Bayon, G., Burton, K., 2002. Hf isotope ratio analysis using multi-collector inductively coupled plasma mass spectrometry: an evaluation of isobaric interference corrections. Journal of Analytical Atomic Spectrometry 17, 1567–1574.

Clemens, J.D., Stevens, G., Farina, F., 2011. The enigmatic sources of I-type granites: The peritectic connexion. Lithos 126, 174–181.

Clift, P., Vannucchi, P., 2004. Controls on tectonic accretion versus erosion in subduction zones: Implications for the origin and recycling of the continental crust. Reviews of Geophysics 42, RG2001.

Cochrane, R., Spikings, R., Gerdes, A., Ulianov, A., Mora, A., Villagómez, D., Putlitz, B., Chiaradia, M., 2014a. Permo-Triassic anatexis, continental rifting and the disassembly of western Pangaea. Lithos.

Cochrane, R., Spikings, R., Gerdes, A., Winkler, W., Ulianov, A., Mora, A., Chiaradia, M., 2014b. Distinguishing between in-situ and accretionary growth of continents along active margins. Lithos 202, 382–394.

Cocks, L.R.M., Torsvik, T.H., 2002. Earth geography from 500 to 400 million years ago: a faunal and palaeomagnetic review. Journal of the Geological Society 159, 631–644.

Collins, W.J., 2002. Hot orogens, tectonic switching, and creation of continental crust. Geology 30, 535.

Collins, W.J., Belousova, E.A., Kemp, A.I.S., Murphy, J.B., 2011. Two contrasting Phanerozoic orogenic systems revealed by hafnium isotope data. Nature Geoscience 4, 333–337.

Collins, W.J., Richards, S.W., 2008. Geodynamic significance of S-type granites in circum-Pacific orogens. Geology 36, 559–562.

Cordani, U.G., Cardona, A., Jimenez, D.M., Liu, D., Nutman, A.P., 2005. Geochronology of Proterozoic basement inliers in the Colombian Andes: Tectonic history of remnants of a fragmented Grenville belt. Geological Society, London, Special Publications 246, 329–346.

Dahlquist, J.A., Pankhurst, R.J., Gaschnig, R.M., Rapela, C.W., Casquet, C., Alasino, P.H., Galindo, C., Baldo, E.G., 2012. Hf and Nd isotopes in Early Ordovician to Early Carboniferous granites as monitors of crustal growth in the Proto-Andean margin of Gondwana. Gondwana Research.

Dalziel, I.W.D., 1986. Collision and Cordilleran orogenesis: an Andean perspective. Geological Society, London, Special Publications 19, 389–404.

Davidson, J.P., Arculus, R.J., 2006. The significance of Phanerozoic arc magmatism in generating continental crust, in: Brown, M., Rushmer, T. (Eds.), Evolution and Differentiation of the Continental Crust. Cambridge University Press, pp. 135–172.

Feo-Codecido, G., Smith Jr, F.D., Aboud, N., Di Giacomo, E., 1984. Basement and Paleozoic rocks of the Venezuelan Llanos basins. Geological Society of America, Memoir 162, 173–187.

Fyfe, W.S., 1978. The evolution of the Earth's crust: Modern plate tectonics to ancient hot spot tectonics? Chemical Geology 23, 89–114.

García, C., Ríos, C., Castellanos, Ó.M.A., 2005. Medium-pressure metamorphism of the Silgará Formation in the central Santander Massif, Eastern Cordillera, Colombian Andes: constraints for a collision model. Boletín de Geología, Universidad Industrial de Santander 27, 43–68.

Gerdes, A., Zeh, A., 2006. Combined U–Pb and Hf isotope LA-(MC-) ICP-MS analyses of detrital zircons: comparison with SHRIMP and new constraints for the provenance and age of an Armorican metasediment in Central Germany. Earth and Planetary Science Letters 249, 47–61.

Goldsmith, R., Marvin, R.F., Mehnert, H.H., 1971. Radiometric ages in the Santander Massif, eastern Cordillera, Colombian Andes. United States Geological Survey Professional Paper 750, 44–49.

Gómez, J., Nivia, A., Montes, N.E., Jiménez, D.M., Sepúlveda, J., Gaona, T., Osorio, J., Diederix, H., Mora, M., Velásquez, M., 2007. Atlas geológico de Colombia 1:500'000.

Gonzales de Juana, C., de Arozena, J.M.., Cadillat, X.P., 1980. Geología de Venezuela y de sus Cuencas Petrolíferas. Foninves, Caracas.

Grauch, R.I., 1972. Preliminary report of a Late (?) Paleozoic metamorphic event in the Venezuelan Andes. Geological Society of America Memoir 132, 465–473.

Gutscher, M.A., 2002. Andean subduction styles and their effect on thermal structure and interplate coupling. Journal of South American Earth Sciences 15, 3–10.

Hackley, P.C., Urbani, F., Karlsen, A.W., Garrity, P., 2005. Geologic Shaded Relief Map of Venezuela. Open-file report, USGS.

Harris, C., Faure, K., Diamond, R.E., Scheepers, R., 1997. Oxygen and hydrogen isotope geochemistry of S-and I-type granitoids: the Cape Granite suite, South Africa. Chemical Geology 143, 95–114.

Hauser, N., Matteini, M., Omarini, R.H., Pimentel, M.M., 2011. Combined U–Pb and Lu–Hf isotope data on turbidites of the Paleozoic basement of NW Argentina and petrology of associated igneous rocks: Implications for the tectonic evolution of western Gondwana between 560 and 460Ma. Gondwana Research 19, 100–127.

Hawkesworth, C.J., Kemp, A.I.S., 2006. Using hafnium and oxygen isotopes in zircons to unravel the record of crustal evolution. Chemical Geology 226, 144–162.

Hoorn, C., Guerrero, J., Sarmiento, G.A., Lorente, M.A., 1995. Andean tectonics as a cause for changing drainage patterns in Miocene northern South America. Geology 23, 237–240.

Huppert, H.E., Sparks, R.S.J., 1988. The generation of granitic magmas by intrusion of basalt into continental crust. Journal of Petrology 29, 599–624.

Ibañez-Mejia, M., Pullen, A., Arenstein, J., Gehrels, G.E., Valley, J., Ducea, M.N., Mora, A.R., Pecha, M., Ruiz, J., 2015. Unraveling crustal growth and reworking processes in complex zircons from orogenic lower-crust: The Proterozoic Putumayo Orogen of Amazonia. Precambrian Research 267, 285–310.

Ibañez-Mejia, M., Ruiz, J., Valencia, V.A., Cardona, A., Gehrels, G.E., Mora, A.R., 2011. The Putumayo Orogen of Amazonia and its implications for Rodinia reconstructions: New U–Pb geochronological insights into the Proterozoic tectonic evolution of northwestern South America. Precambrian Research 191, 58–77.

Jull, M., Kelemen, P.B., 2001. On the conditions for lower crustal convective instability. Journal of Geophysical Research 106, 6423–6446.

Kammer, A., Sánchez, J., 2006. Early Jurassic rift structures associated with the Soapaga and Boyaca faults of the Eastern Cordillera, Colombia: Sedimentological inferences and regional implications. Journal of South American Earth Sciences 21, 412–422.

Kemp, A.I.S., Hawkesworth, C.J., Collins, W.J., Gray, C.M., Blevin, P.L., 2009. Isotopic evidence for rapid continental growth in an extensional accretionary orogen: The Tasmanides, eastern Australia. Earth and Planetary Science Letters 284, 455–466.

Kovach, A., Hurley, P.M., Fairbairn, H.W., 1977. Rb-Sr Whole Rock Dating of Metamorphic Events in the Iglesias Complex, Venezuelan Andes. The Journal of Geology 85, 372–377.

Liew, T.C., Hofmann, A.W., 1988. Precambrian crustal components, plutonic associations, plate environment of the Hercynian Fold Belt of central Europe: indications from a Nd and Sr isotopic study. Contributions to Mineralogy and Petrology 98, 129–138.

Lucassen, F., Franz, G., 2005. The Early Palaeozoic Orogen in the Central Andes: a non-collisional orogen comparable to the Cenozoic high plateau? Geological Society, London, Special Publications 246, 257–273.

Maniar, P.D., Piccoli, P.M., 1989. Tectonic discrimination of granitoids. Geological Society of America Bulletin 101, 635–643.

Mantilla-Figueroa, L.C., Bissig, T., Cottle, J.M., Hart, C.J.R., 2012. Remains of early Ordovician mantle-derived magmatism in the Santander Massif (Colombian Eastern Cordillera). Journal of South American Earth Sciences 38, 1–12.

Mantilla-Figueroa, L.C., García-Ramírez, C.A., Valencia, V.A., 2016. A proposal to split-off the so-called "Silgará Formation" (Santander Massif, Colombia) supported on detrital U-Pb zircon ages. Boletin de Geología 38, 33–50.

Mišković, A., Schaltegger, U., 2009. Crustal growth along a non-collisional cratonic margin: a Lu–Hf isotopic survey of the Eastern Cordilleran granitoids of Peru. Earth and Planetary Science Letters 279, 303–315.

Moreno-Sánchez, M., Toro-Toro, L.M., Gómez-Cruz, A., Ruiz, E.C., 2016. Formación Nogontova, una nueva unidad litoestratigráfica en la Cordillera Oriental de Colombia. Boletín de Geología 38.

Nandedkar, R., Hürlimann, N., Ulmer, P., Müntener, O., 2012. Granitic liquids derived by fractional crystallization: an experimental liquid line of decent from olivine-tholeiite to granite at 0.7 GPa. Presented at the EGU General Assembly, p. 5105.

Odremán, O., Useche, A., 1997. Léxico Estratigráfico de Venezuela, Boletin de Geologia, Publicación Especial No. 12. Caracas, Venezuela.

Ordóñez-Carmona, O., Restrepo Álvarez, J.J., Pimentel, M.M., 2006. Geochronological and isotopical review of pre-Devonian crustal basement of the Colombian Andes. Journal of South American Earth Sciences 21, 372–382.

Ostos, M., Yoris, F., Lallemant, H.G.A., 2005. Overview of the southeast Caribbean–South American plate boundary zone. Geological Society of America Special Papers 394, 53–89.

Petford, N., Cruden, A.R., McCaffrey, K.J.W., Vigneresse, J.L., 2000. Granite magma formation, transport and emplacement in the Earth's crust. Nature 408, 669–673.

Pitcher, W.S., 1997. The nature and origin of granite. Springer.

Ramos, V.A., 2009. Anatomy and global context of the Andes: Main geologic features and the Andean orogenic cycle. Backbone of the Americas: Shallow Subduction, Plateau Uplift, and Ridge and Terrane Collision: Geological Society of America Memoir 204, 31–65.

Reimann, C.R., Bahlburg, H., Kooijman, E., Berndt, J., Gerdes, A., Carlotto, V., López, S., 2010. Geodynamic evolution of the early Paleozoic Western Gondwana margin 14–17 S reflected by the detritus of the Devonian and Ordovician basins of southern Peru and northern Bolivia. Gondwana Research 18, 370–384.

Restrepo-Pace, P.A., 1995. Late Precambrian to Early Mesozoic tectonic evolution of the Colombian Andes, based on new geochronological geochemical and isotopic data. (PhD Thesis, University of Arizona, USA).

Restrepo-Pace, P.A., Cediel, F., 2010. Northern South America basement tectonics and implications for paleocontinental reconstructions of the Americas. Journal of South American Earth Sciences 29, 764–771.

Ríos, C., García, C., Takasu, A., 2003. Tectono-metamorphic evolution of the Silgará Formation metamorphic rocks in the southwestern Santander Massif, Colombian Andes. Journal of South American Earth Sciences 16, 133–154.

Roberts, M.P., Clemens, J.D., 1993. Origin of high-potassium, calc-alkaline, I-type granitoids. Geology 21, 825–828.

Rollinson, H.R., 1993. Using geochemical data: evaluation, presentation, interpretation. Prentice-Hall, Essex, England.

Rudnick, R.L., Fountain, D.M., 1995. Nature and composition of the continental crust: a lower crustal perspective. Reviews of Geophysics 33, 267–309.

Schandl, E.S., Gorton, M.P., 2002. Application of high field strength elements to discriminate tectonic settings in VMS environments. Economic Geology 97, 629–642.

Spear, F.S., 1993. Metamorphic phase equilibria and pressure-temperature-time paths, Mineralogical Society of America Monograph. Mineralogical Society of America, Washington.

Spear, F.S., Kohn, M.J., Cheney, J.T., 1999. P-T paths from anatectic pelites. Contributions to Mineralogy and Petrology 134, 17–32.

Spikings, R., Cochrane, R., Villagomez, D., Van der Lelij, R., Vallejo, C., Winkler, W., Beate, B., 2015. The geological history of northwestern South America: from Pangaea to the early collision of the Caribbean Large Igneous Province (290–75Ma). Gondwana Research 27, 95–139.

Staargaard, C.F., Carlson, G.C., 2000. The Bailadores volcanogenic massive sulphide deposit, Venezuela, in: Sherlock, R.L., Logan, M.A. (Eds.), Volcanogenic Massive Sulphide Deposits of Latin America, Geological Association of Canada Special Publication. pp. 315–323.

Stern, R.J., Scholl, D.W., 2010. Yin and yang of continental crust creation and destruction by plate tectonic processes. International Geology Review 52, 1–31.

Thompson, A.B., Connolly, J.A., 1995. Melting of the continental crust: Some thermal and petrological constraints on anatexis in continental collision zones and other tectonic settings. Journal of Geophysical Research 100, 15565–15580.

Urueña-Suárez, C.L., Zuluaga, C.A., 2011. Petrography of the Bucaramanga Gneiss near to Cepita, Berlin and Vetas - Santander. Geología Colombiana 36, 37–56.

van der Lelij, R., Spikings, R., Mora, A., 2016a. Thermochronology and tectonics of the Mérida Andes and the Santander Massif, NW South America. Lithos 248, 220–239.

van der Lelij, R., Spikings, R., Ulianov, A., Chiaradia, M., Mora, A., 2016b. Palaeozoic to Early Jurassic history of the northwestern corner of Gondwana, and implications for the evolution of the Iapetus, Rheic and Pacific Oceans. Gondwana Research 31, 271–294. https://doi.org/10.1016/j.gr.2015.01.011

Vervoort, J.D., Patchett, P.J., 1996. Behavior of hafnium and neodymium isotopes in the crust: constraints from Precambrian crustally derived granites. Geochimica et Cosmochimica Acta 60, 3717–3733.

Vervoort, J.D., Patchett, P.J., Blichert-Toft, J., Albarède, F., 1999. Relationships between Lu–Hf and Sm–Nd isotopic systems in the global sedimentary system. Earth and Planetary Science Letters 168, 79–99.

Villagómez, D., Spikings, R., Mora, A., Guzmán, G., Ojeda, G., Cortés, E., van der Lelij, R., 2011. Vertical tectonics at a continental crust-oceanic plateau plate boundary zone: Fission track thermochronology of the Sierra Nevada de Santa Marta, Colombia. Tectonics 30.

Ward, D.E., Goldsmith, R., Jaime, B., Restrepo, H.A., 1974. Geology of quadrangles H-12, H-13, and parts of I-12 and I-13, (zone III) in northeastern Santander Department, Colombia, Open-File Report 74-258. U.S. Geological Survey.

Weber, B., Iriondo, A., Premo, W.R., Hecht, L., Schaaf, P., 2007. New insights into the history and origin of the southern Maya block, SE México: U–Pb–SHRIMP zircon geochronology from metamorphic rocks of the Chiapas massif. International Journal of Earth Sciences 96, 253–269.

Weber, B., Scherer, E.E., Schulze, C., Valencia, V.A., Montecinos, P., Mezger, K., Ruiz, J., 2010. U–Pb and Lu–Hf isotope systematics of lower crust from central-southern Mexico–Geodynamic significance of Oaxaquia in a Rodinia Realm. Precambrian Research 182, 149–162.

Willbold, M., Stracke, A., 2010. Formation of enriched mantle components by recycling of upper and lower continental crust. Chemical Geology 276, 188–197.

Willner, A.P., Gerdes, A., Massonne, H.-J., 2008. History of crustal growth and recycling at the Pacific convergent margin of South America at latitudes 29–36 S revealed by a U–Pb and Lu–Hf isotope study of detrital zircon from late Paleozoic accretionary systems. Chemical Geology 253, 114–129.

Zindler, A., Hart, S.R., 1986. Chemical geodynamics. Annual Reviews of Earth and Planetary Sciences 14, 493–571.

Figure Captions

Figure 1: Digital relief map (Amante and Eakins, 2008) showing the tectonic provinces of northern South America modified from Feo-Codecido et al. (1984) and Ostos et al. (2005). The ranges of geological maps in Figures 2 and 3 are highlighted in dashed red boxes. BB: Bonaire Block, CC: Central Cordillera, CM: EC: Eastern Cordillera, GM: Garzón Massif, MA: Mérida Andes, PP: Paraguana Peninsuala, SM: Santander Massif, SNSM: Sierra Nevada de Santa Marta, SP: Sierra del Perijá, TI: Toas Island.

Figure 2: Geological map of the Mérida Andes, Venezuela, simplified and modified from Hackley et al. (2005). Locations of all analysed samples are shown. Sample codes in parentheses (XX) correspond to full sample codes 08VDLXX. All quoted ages are weighted mean zircon ^{238}U-^{206}Pb dates with uncertainties at the 2σ confidence level (Van der Lelij et al., 2016b) are marked in bold text. Semibold text beneath the sample age indicates εHf_t ±2σ, regular text indicates the sample's whole rock εNd_t without uncertainties, and numbers in italic are whole rock $^{87}Sr/^{86}Sr_i$ ratios.

Figure 3: Geological map of the Santander Massif, Colombia, simplified and modified from Gómez et al. (2007). Sample codes in parentheses (XX) correspond to full sample codes 10VDLXX. All quoted ages are weighted mean zircon ^{238}U-^{206}Pb dates with uncertainties at the 2σ confidence level (Van der Lelij et al., 2016b) are marked in bold text. Semibold text beneath the sample age indicates εHf_t ±2σ, regular text indicates the sample's whole rock εNd_t without uncertainties, and numbers in italic are whole rock $^{87}Sr/^{86}Sr_i$ ratios.

Figure 4: Simplified stratigraphic summary of the Mérida Andes and the Santander Massif based on a compilation of data from Van der Lelij et al., 2016. Igneous activity and tectonic regimes are broadly similar and are considered together for both regions, and are labelled in pink for periods of compression and blue for periods of extension.

Figure 5: Graphical summary of all isotopic data collected during this study from rocks yielding zircon U-Pb crystallisation ages that range between 499 and 415 Ma. The vertical lines at 472, 452 and 442 Ma indicate interpreted times of changing tectonic regimes. Crustal evolution lines are shown for the Lu-Hf isotopic system for an average crustal $^{176}Lu/^{177}Hf$ ratio of 0.0113 (Gerdes and Zeh, 2006 and references therein), and are labelled according to their corresponding model age. Colour coding is identical for all graphs, and shown in the inset. All uncertainties are quoted at the 2σ level.

Figure 6: Graphical summary of all isotopic data collected during this study from rocks yielding zircon U-Pb crystallisation ages between ~272 and ~196 Ma. Crustal evolution lines are shown for the Lu-Hf isotopic system for an average crustal $^{176}Lu/^{177}Hf$ ratio of 0.0113 (Gerdes and Zeh, 2006 and references therein), and are labelled according to their corresponding model age. Colour coding is identical for all graphs, and shown in the inset. All uncertainties are quoted at the 2σ level.

Figure 7: Plot of εHf_t (zircon) vs. εNd_t (whole rock). All uncertainties are plotted at the 2σ level. The labelled oblique lines are best-fit regressions across large compiled datasets from Vervoort et al. (1999). Sample 08VDL11 is labelled. See text for discussion.

Figure 8: Geochemical and isotopic correlation plots comparing Lu-Hf model ages with whole rock initial $^{87}Sr/^{86}Sr_i$ ratios, whole rock alumina saturation index A/CNK (Maniar and Piccoli, 1989) and quartz $\delta^{18}O$ (‰).

Figure 9: Schematic cross-section for the Palaeozoic evolution of the northern Andes based on this study and on results described in Van der Lelij et al., 2016. See text for discussion. CB: Caparo Block, MA: Mérida Andes; SM: Santander Massif. Cardinal directions are in present day coordinates.

Table 1: Summary of isotopic data obtained during this study. All uncertainties are quoted at the 2σ level. TDM-Hf: two stage Lu-Hf model age; TDM-Nd: two stage Sm-Nd model age, $^{87}Sr/^{86}Sr_i$: initial calculated strontium isotopic composition, A/CNK: Alumina Saturation Index (Maniar and Piccoli, 1989). Values in italic are considered to be unreliable and are included for reference only.See methods section for details.

Table 1

Sample data		Coordinates		Zircon U-Pb			Zircon Lu-Hf data			Whole rock	Whole rock Sm-Nd data				Whole rock Rb-Sr data			Quartz
Sample	Unit	Latitude N	Longitude W	Age (Ma)	±2σ	Th/U	εHf_t	2σ	TDM-Hf (Ga)	A/CNK	εNd	εNd_t	±2σ	TDM-Nd (Ga)	$^{87}Rb/^{86}Sr$	$^{87}Sr/^{86}Sr$	$^{87}Sr/^{86}Sr_i$	$\delta^{18}O$ (‰)
Mérida Andes																		
08VDL03	Verdalito granodiorite	8°28'49"	71°34'13"	449.3	2.5	0.34	-2.10	0.26	1.19	1.08	-7.75	-3.27	0.04	1.39	2.6093	0.7255	0.7088	11.30
08VDL04	Pueblo Hondo granite	8°17'53"	71°53'58"	434.2	4.4	1.02	0.30	0.71	1.01	1.08	-7.96	-1.76	0.11	1.26	1.1204	0.7136	0.7067	9.56
08VDL11A	Micarache Orthogneiss protolith	8°41'41"	70°53'31"	1008.6	6.7	0.34	3.20	0.83	1.37	1.17	-6.88	3.54	0.09	1.31				
08VDL11B	Micarache Orthogneiss anatexis			454.0	10.0	0.97	3.06	4.7	0.95									
08VDL14	El Carmen granodiorite	8°45'07"	70°57'33"	211.2	1.2	0.40	-2.60	0.28	0.93	1.20	-6.34	-4.32	0.09	1.29	0.5577	0.7110	0.7093	11.03
08VDL15	Bailadores alkali rhyolite tuff	8°11'51"	71°50'09"	452.6	2.7	0.56	4.50	0.31	0.82	1.16	-1.71	1.58	0.12	1.02	6.9739	0.7504	0.7054	
08VDL18	La Quinta rhyodacite	8°08'56"	72°00'55"	202.0	1.6	0.78	-5.76	0.69	1.19	1.24								
08VDL21	La Grita Diorite	8°08'28"	71°56'15"	471.8	4.0	0.91	0.08	0.34	1.08	0.93	-5.33	-0.21	0.06	1.17	0.4163	0.7081	0.7053	
08VDL22	La Playita orthogneiss	8°11'38"	71°53'02"	449.7	4.4	0.48	-3.79	0.44	1.28	1.28	-7.53	-4.06	0.14	1.46	6.4036	0.7470	0.7059	
08VDL23	Mucubaji granite	8°48'36"	70°48'47"	237.1	1.4	0.12	-4.90	2.10	1.16	1.27								
08VDL26	Mitisus striped gneiss	8°52'31"	70°37'48"	488.2	4.3	0.36	-8.35	0.59	1.56									
08VDL27	La Raya granitic gneiss	8°51'34"	70°34'51"	488.5	6.5	0.38	-8.61	0.53	1.57	1.30	-8.57	-7.15	0.23	1.73				
08VDL32	La Soledad granodiorite	8°49'48"	70°31'47"	414.5	3.9	0.36	-1.10	0.40	1.10	1.20	-6.73	-3.14	0.05	1.36	3.9653	0.7335	0.7101	10.27
08VDL35	Cerro Azul granodiorite	8°53'14"	70°23'34"	499.4	2.7	0.81	-7.70	0.27	1.53	1.19	-9.44	-5.67	0.07	1.62	0.8218	0.7156	0.7098	11.42
08VDL36	Puente Real augen gneiss	8°27'53"	71°26'50"	472.3	3.4	0.59	-7.30	0.33	1.49									
08VDL38	Macanas alkali granite	8°20'19"	71°37'21"	454.8	4.2	0.60	-0.10	0.60	1.07	1.26	-4.78	-1.26	0.29	1.24	*11.4075*	*0.7749*	*0.7010*	
08VDL4	La Culata granodiorite	8°48'27"	71°00'04"	213.	1.	0.3	-4.	0.	1.1	1.30	-7.	-5.	0.	1.3	0.827	0.710	0.708	10.66

0		"		2	7	2	1	2	1		6	4	0	8	2	6	1		
							8	2			0	2	5						
							-	0			-	-	0						
08V		8°5		45	3	0.	2.	.	1.		9.	5.	.	1.	12.	0.7	0.7		
DL4	Chachopo	5'55	70°4	4.	.	2	4	4	2		6	3	0	5	89	97	13	14.	
1	granite	"	7'31"	5	1	9	0	2	1	1.34	7	9	7	6	95	2	7	27	
							-	0			-	-	0						
08V		9°1		46	2	0.	1.	.	1.		8.	3.	.	1.	5.0	0.7	0.7		
DL4	Miraflores	0'42	70°3	6.	.	1	6	6	1		1	6	0	4	57	41	07	13.	
4	granodiorite	"	8'08"	8	5	4	0	6	7	1.26	9	1	8	3	2	2	6	51	
							-	0			-	-	0						
08V		9°1		44	1	0.	1.	.	1.		8.	3.	.	1.	2.9	0.7	0.7		
DL4	Valera	1'11	70°3	7.	.	1	7	5	1		6	8	0	4	34	29	11		
5	granodiorite	"	7'51"	9	8	4	3	1	6	1.20	0	2	8	4	3	8	1		
							-	1											
08V	La	9°1		24	3	0.	3.	.	1.										
DL4	Quebrada	0'25	70°3	3.	.	7	9	6	1										
6	granite	"	2'24"	5	4	0	0	0	2	1.42									
							-	0			-	-	0						
08V	Carmania	9°1		45	2	1.	0.	.	1.		7.	1.	.	1.	0.7	0.7	0.7		
DL4	monzodiorit	5'59	70°3	0.	.	1	2	2	0		4	8	0	2	89	11	06		
7	e	"	8'18"	4	5	2	0	3	8	1.03	2	3	7	8	3	2	2		
							-	0			-	-	0						
08V		9°0		45	1	0.	1.	.	1.		7.	3.	.	1.	4.7	0.7	0.7		
DL4	La Puerta	7'11	70°4	3.	.	1	6	7	1		9	3	1	4	28	36	05		
9	granodiorite	"	2'39"	1	8	6	0	5	6	1.19	7	1	1	0	3	3	8		
							-	0			-	-	0						
08V		9°0		44	3	0.	2.	.	1.		7.	3.	.	1.	3.2	0.7	0.7		
DL5	Timotes	0'52	70°4	5.	.	1	7	9	2		8	3	0	4	06	29	09	12.	
0	granite	"	4'25"	2	9	0	3	1	1	1.22	3	7	5	0	7	8	5	07	
								0			-		0						
08V		7°4		47	3	0.	2.	.	0.		5.	0.	.	1.	0.2	0.7	0.7		
DL5	Islitas	9'01	71°2	3.	.	6	3	3	9		2	3	0	1	67	07	05	9.0	
5	tonalite	"	1'01"	1	5	0	2	2	6	1.01	4	0	7	3	3	6	8	3	
											-								
							-	0			1	-	0						
08V		7°5		49	8	0.	7.	.	1.		2.	6.	.	1.	2.9	0.7	0.7		
DL5	El Cambur	2'29	71°1	2.	.	7	9	3	5		1	7	1	7	30	33	12		
6	granite	"	6'03"	3	4	1	9	8	5	1.43	6	3	8	0	4	4	8		
							-	1			-	-	0						
08V		7°5		49	5	0.	2.	.	1.		7.	3.	.	1.	7.5	0.7	0.7		
DL5	El Tapo	1'00	71°1	2.	.	5	5	0	2		7	2	0	4	00	64	11	10.	
7	granite	"	3'41"	3	3	2	0	0	4	1.24	0	2	8	2	4	3	8	34	
Northwestern Venezuela																			
							-	0			-	-	0						
08V		10°		24	1	0.	5.	.	1.		5.	3.	.	1.	1.9	0.7	0.7		
DL5	Toas Island	57'2	71°3	8.	.	6	3	3	2		8	3	3	2	73	12	05		
9	granodiorite	3"	7'45"	9	7	6	7	0	0	1.12	5	1	8	4	8	0	0		
							-	0			-	-	0						
08V	Riecito del	10°		22	1	0.	5.	.	1.		5.	3.	.	1.	0.7	0.7	0.7		
DL6	Palmar	37'5	72°2	5.	.	9	0	3	1		3	0	1	2	02	07	05		
0	granite	6"	1'26"	1	5	0	3	1	6	1.19	9	8	7	1	7	3	1		
							-	0			-	-	0						
08V		11°		27	2	0.	2.	.	1.		5.	2.	.	1.	0.1	0.7	0.7		
DL6	El Amparo	55'5	69°5	2.	.	6	9	2	0		1	2	1	1	74	06	05		
4	diorite	4"	7'36"	2	6	1	0	0	8	0.91	8	0	0	7	0	0	3		
Santander Massif																			
							-	0			-	-	0						
10V		7°0		19	1	0.	5.	.	1.		7.	4.	.	1.	1.6	0.7	0.7		
DL0	Corcova	6'03	73°0	8.	.	7	4	5	1		3	9	1	3	36	13	08		
5	granodiorite	"	0'36"	3	8	7	7	6	6	1.09	7	8	4	3	8	4	8		
							-	0			-	-	0						
10V		6°4		19	1	0.	4.	.	1.		6.	4.	.	1.	1.4	0.7	0.7		
DL2	Pescadero	9'48	72°5	9.	.	8	7	2	1		9	4	1	2	51	12	08		
2	granodiorite	"	9'27"	1	3	8	2	1	2	1.06	3	4	6	9	6	3	2		
								1			-	-	0						
10V		6°5		46	2	0.	0.	.	1.		7.	1.	.	1.	0.2	0.7	0.7		
DL2	Bucaraman	6'35	72°5	1.	.	4	5	0	0		0	0	0	2	36	08	06		
3	ga gneiss	"	8'00"	0	1	9	0	0	5		8	9	5	3	8	1	5		
							-	0											
10V		6°2		20	0	0.	5.	.	1.										
DL2	Onzaga	2'31	72°4	0.	.	8	2	3	1										
8	granodiorite	"	9'06"	4	7	7	1	8	5	1.01									
							-	0											
10V		6°2		20	0	0.	5.	.	1.										
DL3	Onzaga	4'28	72°4	1.	.	7	9	5	1										
1	granodiorite	"	9'08"	0	9	9	3	5	9	1.06									
							-	0											
10V		6°2		19	0	0.	6.	.	1.										
DL3	Mogotes	5'22	72°4	8.	.	8	0	3	1										
2	granodiorite	"	9'29"	0	8	1	8	5	9	1.04									

10V DL35	Rio Surata Diorite	7°10'22"	73°05'08"	20.1	1.4	1.17	-5.75	0.57	1.18	1.11									
10V DL37	Berlin orthogneiss	7°11'24"	72°58'41"	45.1	1.3	0.38	0.76	0.33	1.11	1.05	-7.20	-1.92	0.15	1.29	0.278	0.708	0.706		
10V DL39	Pegmatite from orthogneiss	7°10'46"	72°59'48"	20.1	1.2	0.03	-6.55	0.85	1.24		*-1.20*	*-1.63*	*-3.55*	*1.59*	*4.567*	*0.735*	*0.721*		
10V DL43A	Berlin orthogneiss	7°14'18"	72°49'30"	46.0.3	3.5.3	0.5.3	1.94	0.644	0.97										
10V DL43B	Migmatite in orthogneiss			20.9.2	3.4.2	0.0.2	-2.46	0.300	1.00	1.02	-6.79	-2.16	-0.23	1.32	2.570	0.730	0.713		
10V DL44	Berlin orthogneiss	7°20'40"	72°42'59"	47.3.5	2.5.4	0.2.9	-5.84	0.731	1.41	1.54	-9.94	-5.71	-1.08	1.61	*8.964*	*0.762*	*0.701*		
10V DL46	Pamplona granite	7°16'29"	72°39'55"	43.9.2	4.7.6	0.4.6	5.26	0.447	0.97										
10V DL47	gabbrodiorite	7°28'23"	72°41'44"	48.3.7	5.9.5	0.7.3	-2.73	0.254	1.24	0.80	-7.06	-4.48	-0.68	1.51	1.631	0.724	0.712		
10V DL49	Silgará Fm. Gneiss	7°20'16"	72°42'16"	47.9.8	3.1.0	0.2.0	-6.63	0.386	1.46										
10V DL51	Migmatite from paragneiss	7°15'22"	72°53'45"	47.7.0	5.8.2	0.1.2	-2.10	0.118	1.18	1.08	-7.85	-3.23	-2.21	1.41	3.874	0.735	0.709		
10V DL52	Berlin orthogneiss	7°15'17"	72°53'48"	47.2.5	3.5.4	0.3.0	-6.43	0.314	1.46	1.16	-9.52	-5.30	-1.55	1.57	1.645	0.723	0.712		
10V DL54	Paramo Rico tonalite	7°13'54"	72°53'54"	19.9.8	1.2.7	0.9.1	4.21	0.001	1.15	1.05									
10V DL55	Ocana alkali granite	8°09'45"	73°17'59"	19.5.8	1.8.5	0.0.0	-5.03	0.391	1.13	1.12									
10V DL55	Tarra granodiorite	8°03'10"	73°04'31"	44.3.4	3.4.2	0.4.5	3.12	0.284	1.24	1.09	-8.45	-3.38	-1.14	1.40	1.422	0.718	0.709		
10V DL56	Aguablanca granite	8°07'08"	72°56'51"	20.2.2	1.7.0	0.9.9	5.32	0.262	1.16	1.15									
10V DL58	Bocas Fm. Rhyolite	7°26'27"	73°13'24"	25.0.7	4.0.3	0.8.9	0.00	0.501	0.91	1.18									
10V DL59	Rio Negro tonalite	7°17'13"	73°08'46"	19.6.0	1.2.1	1.2.9	6.11	0.430	1.20	1.05									
10V DL61A	Rio Surata granodiorite enclaves	7°09'59"	73°05'17"	10.18.3	8.0.9	0.3.1	2.85	0.428	1.38										
10V DL61B	Rio Surata granodiorite			20.0.0	1.5.5	1.3.3	-5.48	0.556	1.16	1.13	-9.16	-7.20	-0.09	1.51	0.357	0.717	0.716		

Highlights

- Magmatic sources for granitic rocks vary with changing arc dynamics
- During orogenesis, magmas were typically sourced from older upper crust
- During extension, magmas were typically sourced from younger, lower crust
- There is little evidence for crustal growth along north-western Gondwana between ~500 Ma and ~196 Ma

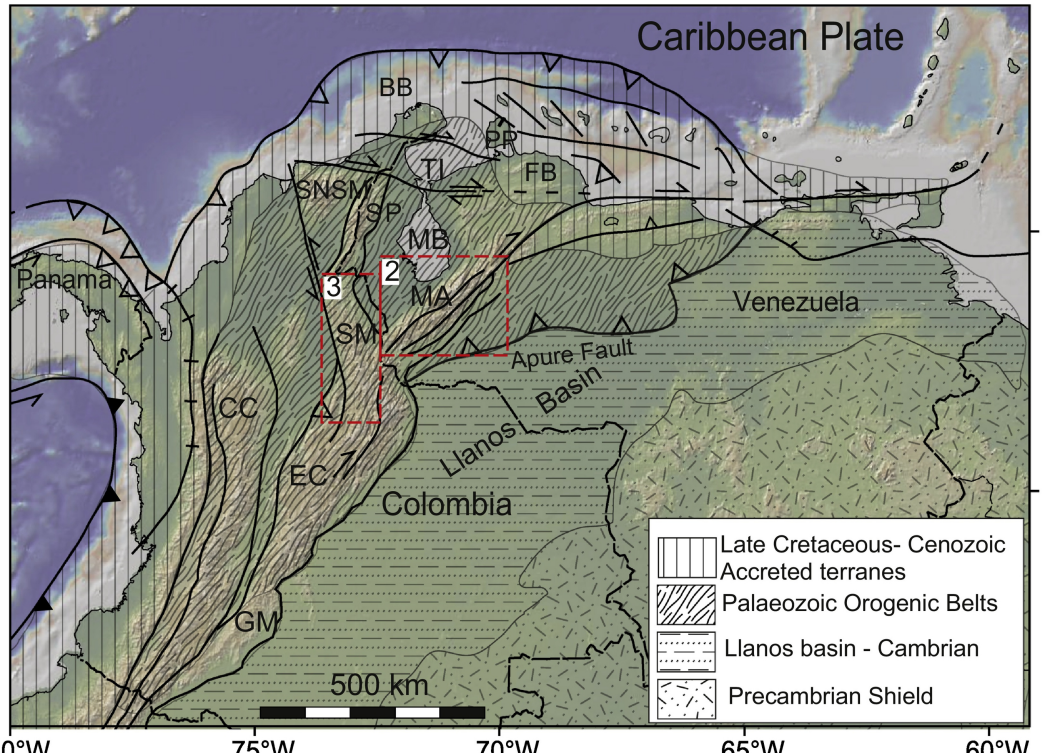
Caribbean Plate
BB
PR
TI
FB
SNSM
SP
MB
MA
SM
CC
EC
GM
Panama
Colombia
Venezuela
Apure Fault
Llanos Basin
2
3
500 km
10°
5°
80°W
75°W
70°W
65°W
60°W
Late Cretaceous- Cenozoic Accreted terranes
Palaeozoic Orogenic Belts
Llanos basin - Cambrian
Precambrian Shield

Figure 1

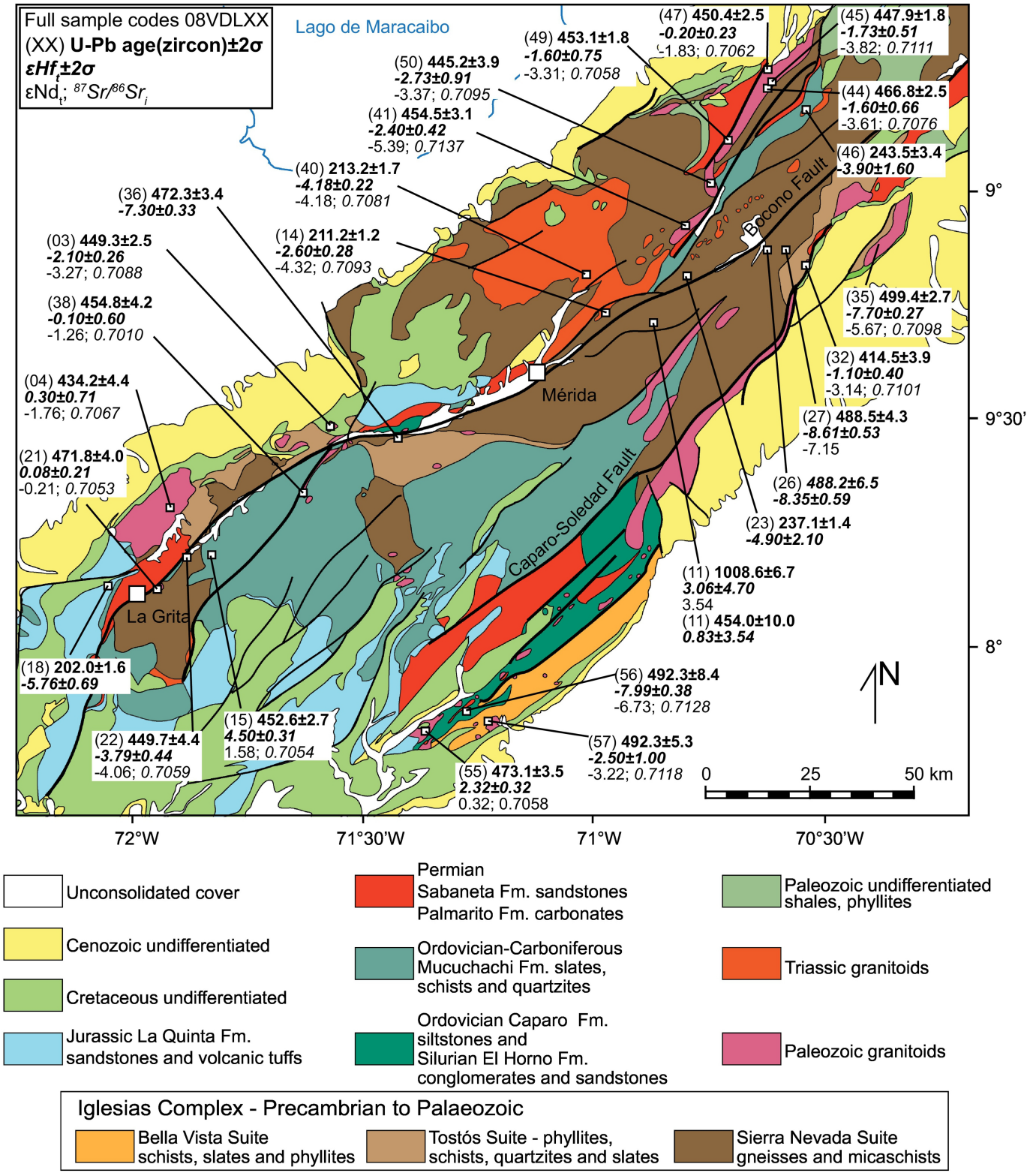
Full sample codes 08VDLXX
(XX) U-Pb age(zircon)±2σ
εHf$_t$±2σ
εNd$_t$; $^{87}Sr/^{86}Sr_i$
Lago de Maracaibo
(47) 450.4±2.5
-0.20±0.23
-1.83; 0.7062
(45) 447.9±1.8
-1.73±0.51
-3.82; 0.7111
(49) 453.1±1.8
-1.60±0.75
-3.31; 0.7058
(50) 445.2±3.9
-2.73±0.91
-3.37; 0.7095
(44) 466.8±2.5
-1.60±0.66
-3.61; 0.7076
(41) 454.5±3.1
-2.40±0.42
-5.39; 0.7137
(46) 243.5±3.4
-3.90±1.60
(40) 213.2±1.7
-4.18±0.22
-4.18; 0.7081
Boconó Fault
(36) 472.3±3.4
-7.30±0.33
(03) 449.3±2.5
-2.10±0.26
-3.27; 0.7088
(14) 211.2±1.2
-2.60±0.28
-4.32; 0.7093
(35) 499.4±2.7
-7.70±0.27
-5.67; 0.7098
(38) 454.8±4.2
-0.10±0.60
-1.26; 0.7010
(32) 414.5±3.9
-1.10±0.40
-3.14; 0.7101
(04) 434.2±4.4
0.30±0.71
-1.76; 0.7067
Mérida
(27) 488.5±4.3
-8.61±0.53
-7.15
(21) 471.8±4.0
0.08±0.21
-0.21; 0.7053
(26) 488.2±6.5
-8.35±0.59
Caparo-Soledad Fault
(23) 237.1±1.4
-4.90±2.10
(11) 1008.6±6.7
3.06±4.70
3.54
(11) 454.0±10.0
0.83±3.54
La Grita
(18) 202.0±1.6
-5.76±0.69
(56) 492.3±8.4
-7.99±0.38
-6.73; 0.7128
(15) 452.6±2.7
4.50±0.31
1.58; 0.7054
(22) 449.7±4.4
-3.79±0.44
-4.06; 0.7059
(57) 492.3±5.3
-2.50±1.00
-3.22; 0.7118
(55) 473.1±3.5
2.32±0.32
0.32; 0.7058
N
0
25
50 km
9°
9°30'
8°
72°W
71°30'W
71°W
70°30'W
Unconsolidated cover
Cenozoic undifferentiated
Cretaceous undifferentiated
Jurassic La Quinta Fm.
sandstones and volcanic tuffs
Permian
Sabaneta Fm. sandstones
Palmarito Fm. carbonates
Ordovician-Carboniferous
Mucuchachi Fm. slates,
schists and quartzites
Ordovician Caparo Fm.
siltstones and
Silurian El Horno Fm.
conglomerates and sandstones
Paleozoic undifferentiated
shales, phyllites
Triassic granitoids
Paleozoic granitoids
Iglesias Complex - Precambrian to Palaeozoic
Bella Vista Suite
schists, slates and phyllites
Tostós Suite - phyllites,
schists, quartzites and slates
Sierra Nevada Suite
gneisses and micaschists

Figure 2

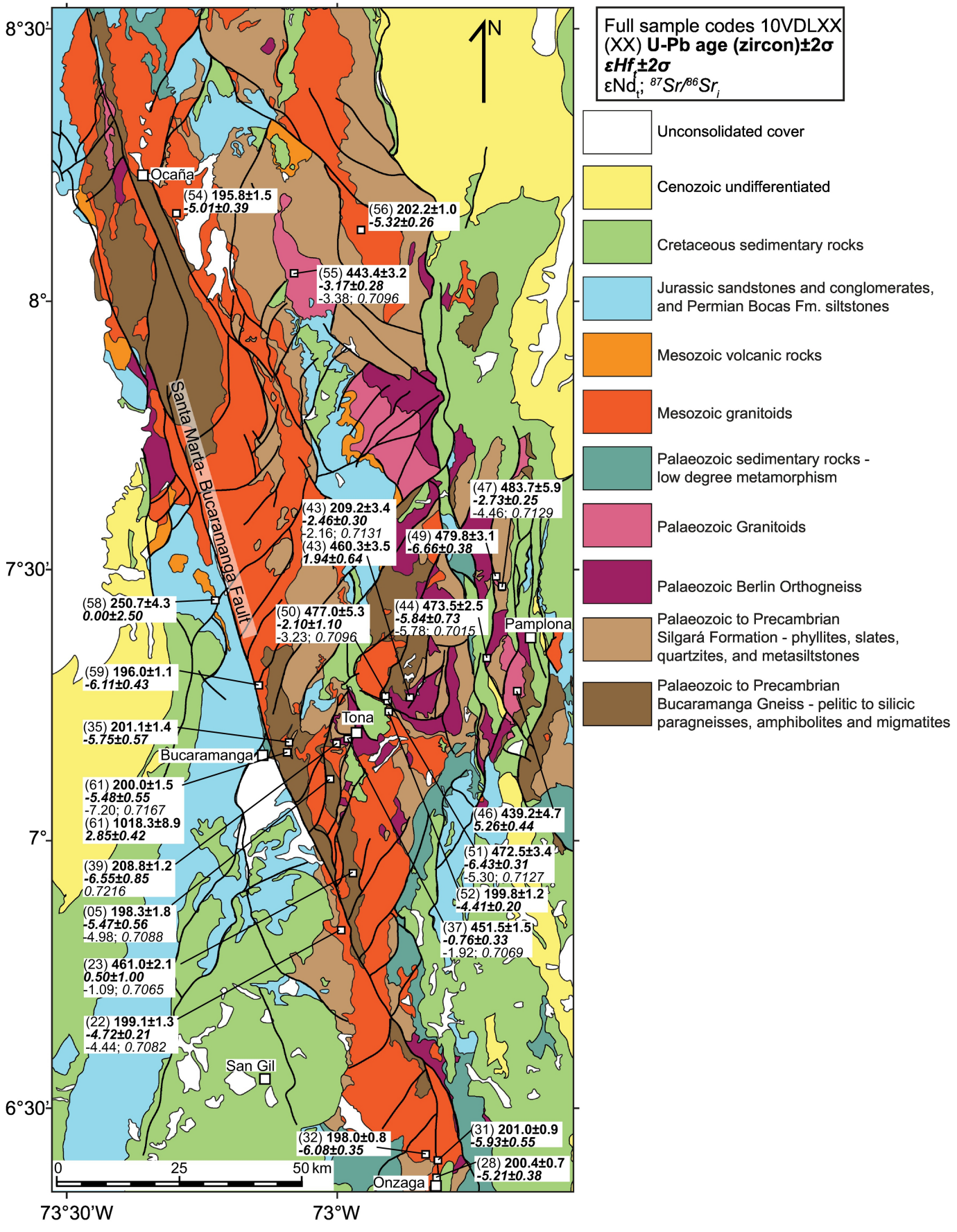
Full sample codes 10VDLXX
(XX) U-Pb age (zircon)±2σ
εHf$_t$±2σ
εNd$_t$; $^{87}Sr/^{86}Sr_i$
Unconsolidated cover
Cenozoic undifferentiated
Cretaceous sedimentary rocks
Jurassic sandstones and conglomerates, and Permian Bocas Fm. siltstones
Mesozoic volcanic rocks
Mesozoic granitoids
Palaeozoic sedimentary rocks - low degree metamorphism
Palaeozoic Granitoids
Palaeozoic Berlin Orthogneiss
Palaeozoic to Precambrian Silgará Formation - phyllites, slates, quartzites, and metasiltstones
Palaeozoic to Precambrian Bucaramanga Gneiss - pelitic to silicic paragneisses, amphibolites and migmatites
N
8°30'
8°
7°30'
7°
6°30'
73°30'W
73°W
0
25
50 km
Ocaña
Santa Marta- Bucaramanga Fault
Pamplona
Tona
Bucaramanga
San Gil
Onzaga
(54) 195.8±1.5
-5.01±0.39
(56) 202.2±1.0
-5.32±0.26
(55) 443.4±3.2
-3.17±0.28
-3.38; 0.7096
(43) 209.2±3.4
-2.46±0.30
-2.16; 0.7131
(43) 460.3±3.5
1.94±0.64
(47) 483.7±5.9
-2.73±0.25
-4.46; 0.7129
(49) 479.8±3.1
-6.66±0.38
(58) 250.7±4.3
0.00±2.50
(50) 477.0±5.3
-2.10±1.10
-3.23; 0.7096
(44) 473.5±2.5
-5.84±0.73
-5.78; 0.7015
(59) 196.0±1.1
-6.11±0.43
(35) 201.1±1.4
-5.75±0.57
(61) 200.0±1.5
-5.48±0.55
-7.20; 0.7167
(61) 1018.3±8.9
2.85±0.42
(46) 439.2±4.7
5.26±0.44
(51) 472.5±3.4
-6.43±0.31
-5.30; 0.7127
(39) 208.8±1.2
-6.55±0.85
0.7216
(52) 199.8±1.2
-4.41±0.20
(05) 198.3±1.8
-5.47±0.56
-4.98; 0.7088
(37) 451.5±1.5
-0.76±0.33
-1.92; 0.7069
(23) 461.0±2.1
0.50±1.00
-1.09; 0.7065
(22) 199.1±1.3
-4.72±0.21
-4.44; 0.7082
(32) 198.0±0.8
-6.08±0.35
(31) 201.0±0.9
-5.93±0.55
(28) 200.4±0.7
-5.21±0.38

Figure 3

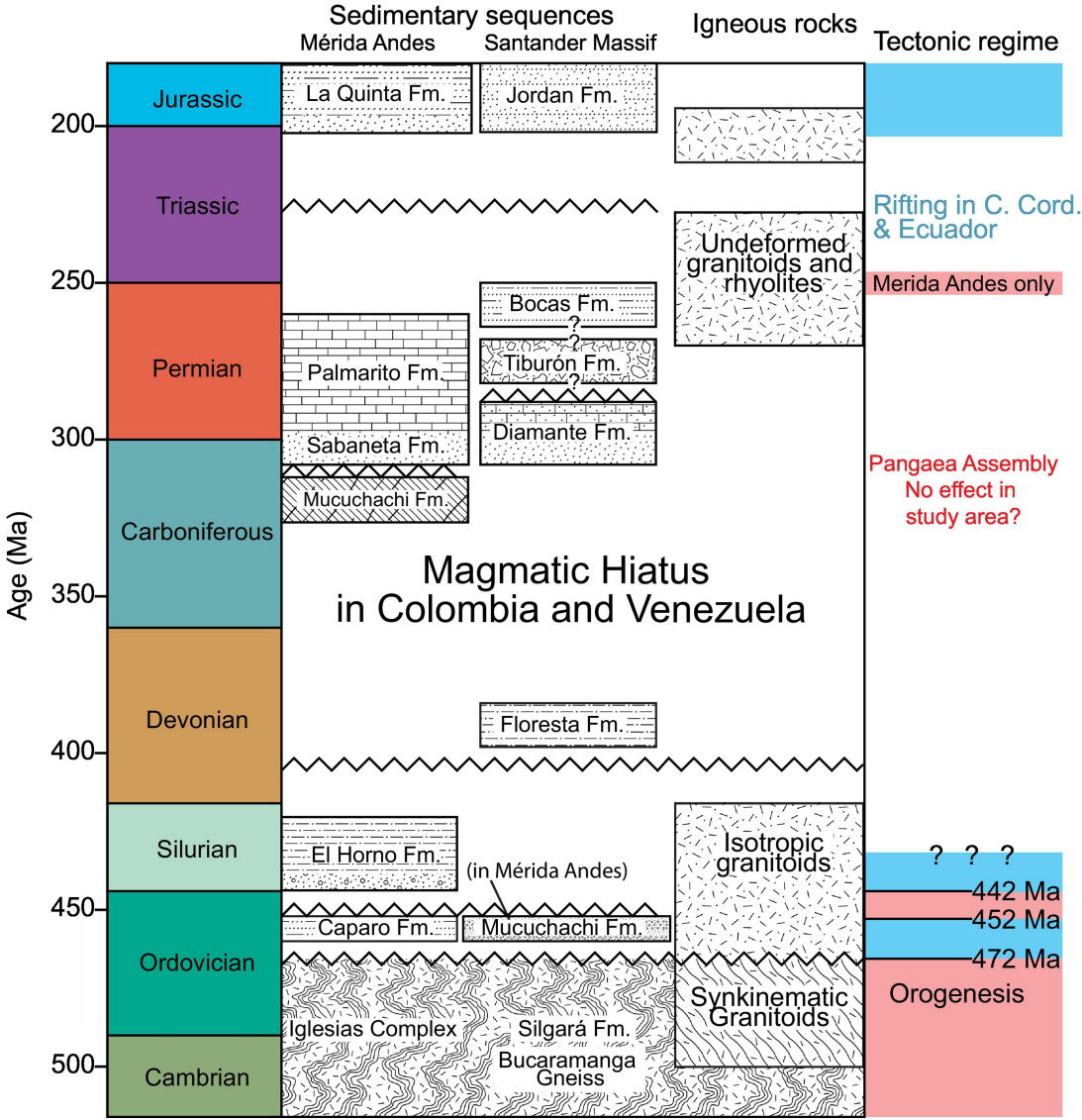
Sedimentary sequences
Mérida Andes
Santander Massif
Igneous rocks
Tectonic regime
Age (Ma)
200
250
300
350
400
450
500
Jurassic
Triassic
Permian
Carboniferous
Devonian
Silurian
Ordovician
Cambrian
La Quinta Fm.
Jordan Fm.
Undeformed granitoids and rhyolites
Rifting in C. Cord. & Ecuador
Merida Andes only
Bocas Fm.
Tiburón Fm.
Palmarito Fm.
Sabaneta Fm.
Diamante Fm.
Mucuchachi Fm.
Pangaea Assembly
No effect in study area?
Magmatic Hiatus
in Colombia and Venezuela
Floresta Fm.
El Horno Fm.
(in Mérida Andes)
Isotropic granitoids
? ? ?
442 Ma
452 Ma
472 Ma
Caparo Fm.
Mucuchachi Fm.
Synkinematic Granitoids
Orogenesis
Iglesias Complex
Silgará Fm.
Bucaramanga Gneiss

Figure 4

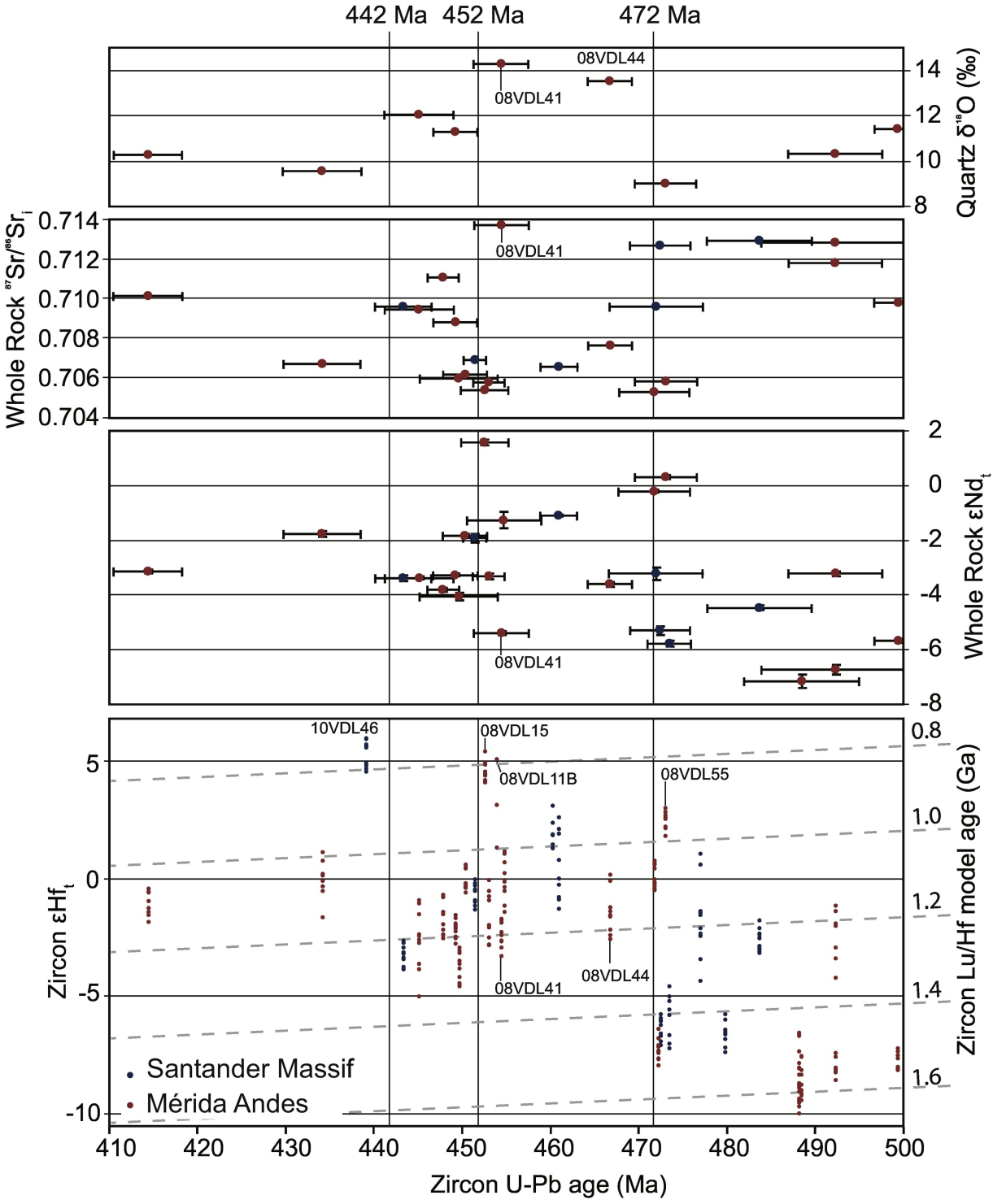
442 Ma
452 Ma
472 Ma
08VDL44
08VDL41
Quartz δ18O (‰)
14
12
10
8
Whole Rock 87Sr/86Sri
0.714
0.712
0.710
0.708
0.706
0.704
Whole Rock εNdt
2
0
-2
-4
-6
-8
10VDL46
08VDL15
08VDL11B
08VDL55
Zircon εHft
5
0
-5
-10
Zircon Lu/Hf model age (Ga)
0.8
1.0
1.2
1.4
1.6
Santander Massif
Mérida Andes
410
420
430
440
450
460
470
480
490
500
Zircon U-Pb age (Ma)

Figure 5

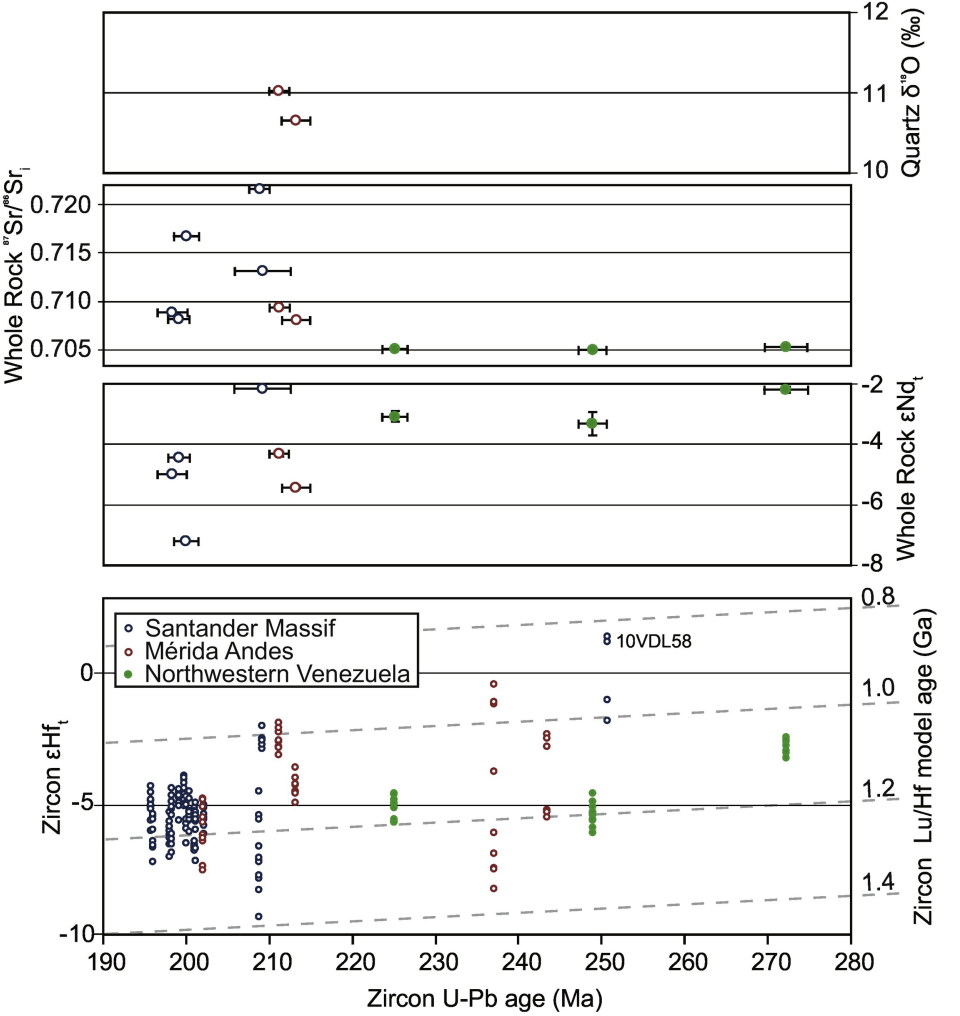
Quartz δ18O (‰)
12
11
10
Whole Rock 87Sr/86Sri
0.720
0.715
0.710
0.705
Whole Rock εNdt
-2
-4
-6
-8
Zircon εHft
0
-5
-10
Zircon Lu/Hf model age (Ga)
0.8
1.0
1.2
1.4
Santander Massif
Mérida Andes
Northwestern Venezuela
10VDL58
190
200
210
220
230
240
250
260
270
280
Zircon U-Pb age (Ma)

Figure 6

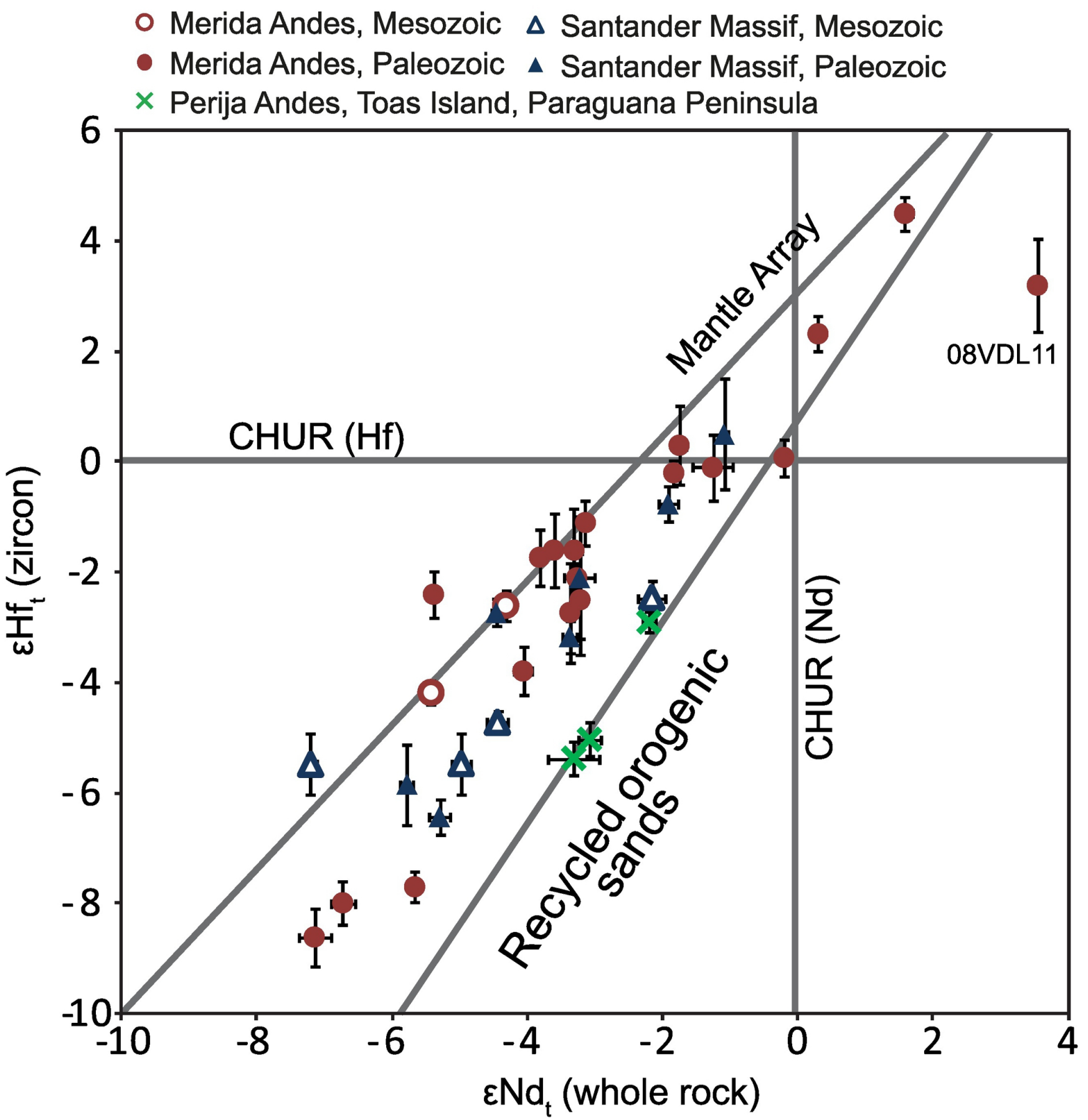
Merida Andes, Mesozoic
Merida Andes, Paleozoic
Perija Andes, Toas Island, Paraguana Peninsula
Santander Massif, Mesozoic
Santander Massif, Paleozoic
Mantle Array
CHUR (Hf)
CHUR (Nd)
Recycled orogenic sands
08VDL11
εHf$_t$ (zircon)
εNd$_t$ (whole rock)
6
4
2
0
-2
-4
-6
-8
-10
-10
-8
-6
-4
-2
0
2
4

Figure 7

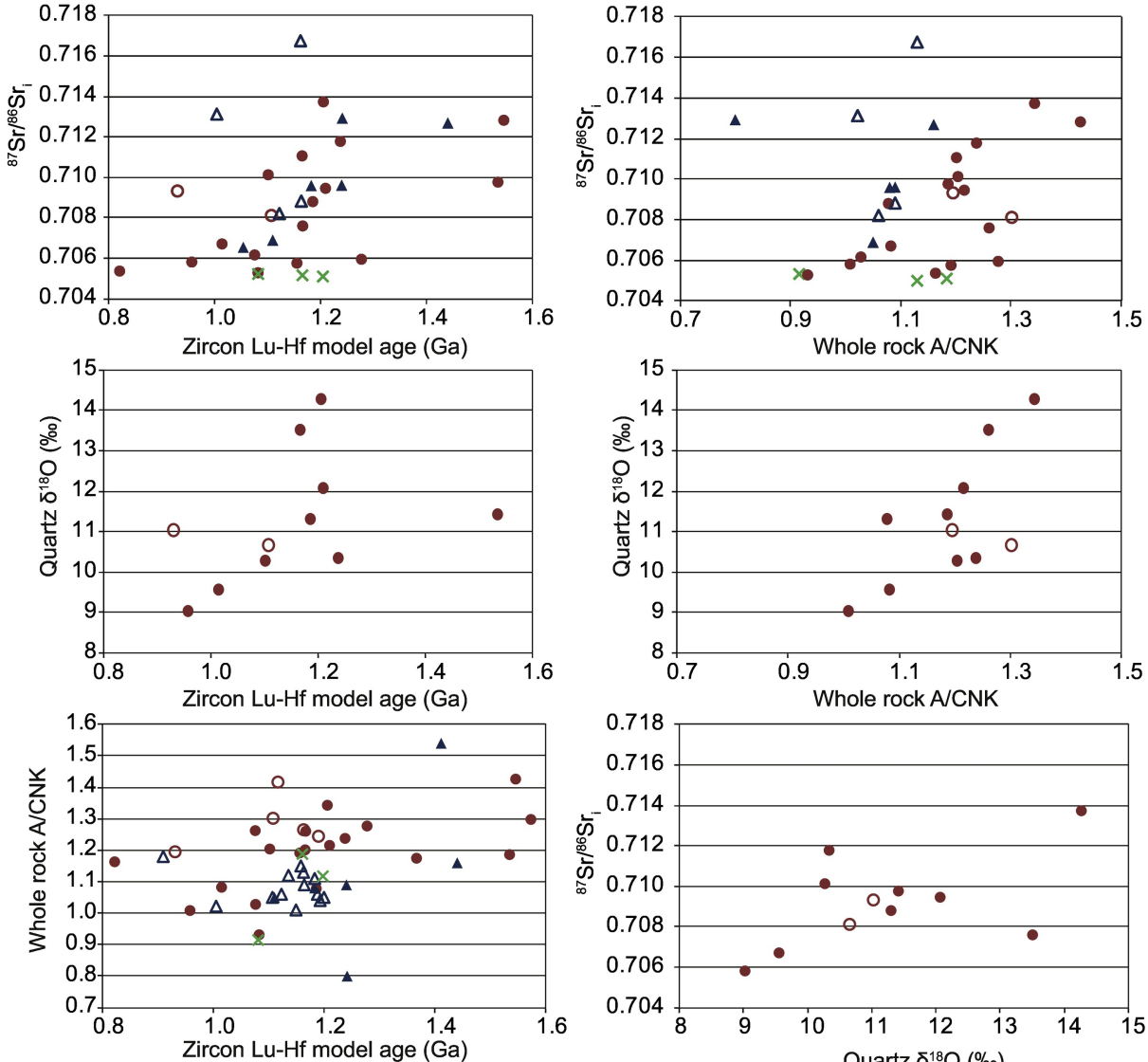
$^{87}Sr/^{86}Sr_i$
Zircon Lu-Hf model age (Ga)
$^{87}Sr/^{86}Sr_i$
Whole rock A/CNK
Quartz $\delta^{18}O$ (‰)
Zircon Lu-Hf model age (Ga)
Quartz $\delta^{18}O$ (‰)
Whole rock A/CNK
Whole rock A/CNK
Zircon Lu-Hf model age (Ga)
$^{87}Sr/^{86}Sr_i$
Quartz $\delta^{18}O$ (‰)
Merida Andes, Mesozoic
Merida Andes, Paleozoic
Perija Andes, Toas Island, Paraguana Peninsula
Santander Massif, Mesozoic
Santander Massif, Paleozoic

Figure 8

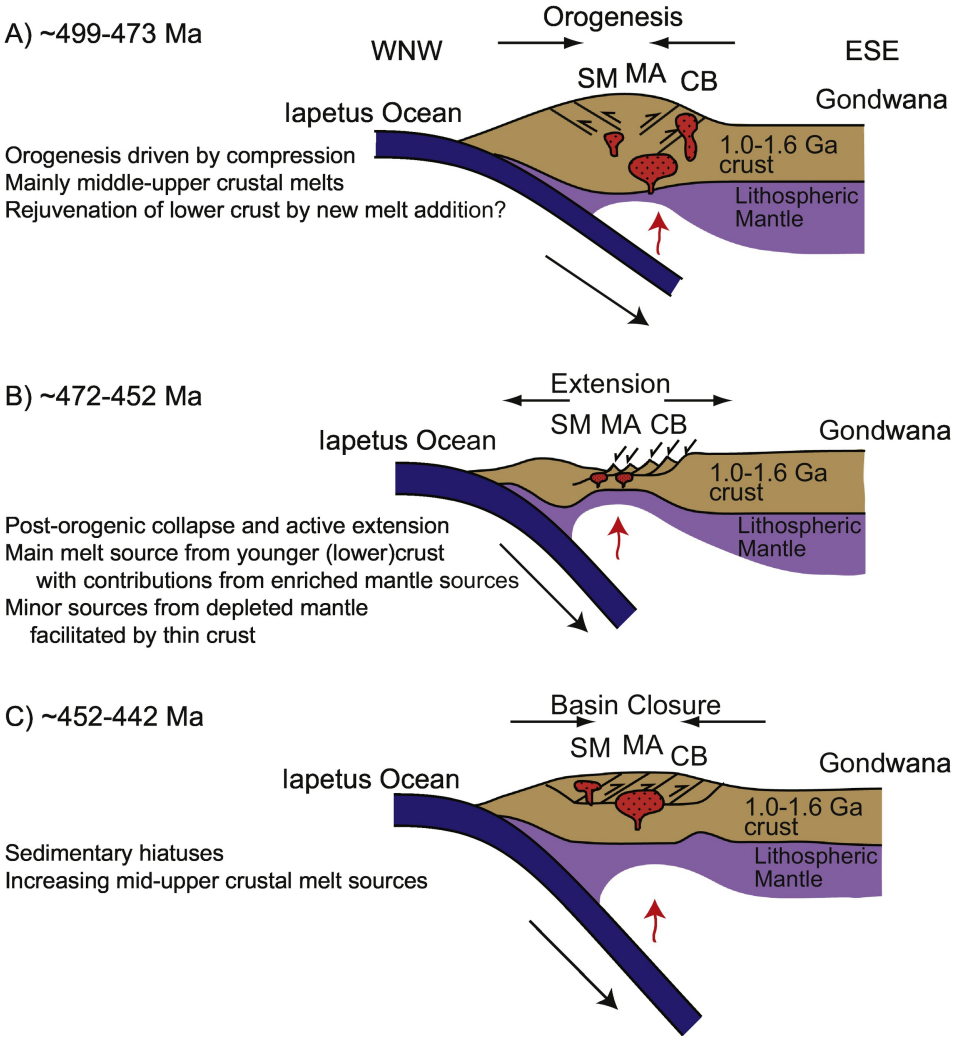
A) ~499-473 Ma
Orogenesis
WNW
ESE
SM MA CB
Gondwana
Iapetus Ocean
1.0-1.6 Ga crust
Lithospheric Mantle
Orogenesis driven by compression
Mainly middle-upper crustal melts
Rejuvenation of lower crust by new melt addition?
B) ~472-452 Ma
Extension
SM MA CB
Iapetus Ocean
Gondwana
1.0-1.6 Ga crust
Lithospheric Mantle
Post-orogenic collapse and active extension
Main melt source from younger (lower)crust
with contributions from enriched mantle sources
Minor sources from depleted mantle
facilitated by thin crust
C) ~452-442 Ma
Basin Closure
SM MA CB
Gondwana
Iapetus Ocean
1.0-1.6 Ga crust
Lithospheric Mantle
Sedimentary hiatuses
Increasing mid-upper crustal melt sources

Figure 9